NAVAL POSTGRADUATE SCHOOL
Monterey, California

THESIS

A FEASIBILITY STUDY OF LIQUID PHASE SINTER FORMING OF A MODEL CERAMIC SYSTEM

by

Roland C. Roeder

March 1999

Co-Advisors: Indranath Dutta
Ashok Gopinath

Approved for public release; distribution is unlimited.

19990517 011

DTIC QUALITY INSPECTED 4

REPORT DOCUMENTATION PAGE	*Form Approved* *OMB No. 0704-0188*

Public reporting burden for this collection of information is estimated to average 1 hour per response, including the time for reviewing instruction, searching existing data sources, gathering and maintaining the data needed, and completing and reviewing the collection of information. Send comments regarding this burden estimate or any other aspect of this collection of information, including suggestions for reducing this burden, to Washington headquarters Services, Directorate for Information Operations and Reports, 1215 Jefferson Davis Highway, Suite 1204, Arlington, VA 22202-4302, and to the Office of Management and Budget, Paperwork Reduction Project (0704-0188) Washington DC 20503.

1. AGENCY USE ONLY *(Leave blank)*	**2. REPORT DATE** March 1999	**3. REPORT TYPE AND DATES COVERED** Master's Thesis

4. TITLE AND SUBTITLE A Feasibility Study of Liquid Phase Sinter Forming of a Model Ceramic System	**5. FUNDING NUMBERS**
6. AUTHOR(S) Roeder, Roland, C.	
7. PERFORMING ORGANIZATION NAME(S) AND ADDRESS(ES) Naval Postgraduate School Monterey, CA 93943-5000	**8. PERFORMING ORGANIZATION REPORT NUMBER**
9. SPONSORING / MONITORING AGENCY NAME(S) AND ADDRESS(ES)	**10. SPONSORING / MONITORING AGENCY REPORT NUMBER**

11. SUPPLEMENTARY NOTES

The views expressed in this thesis are those of the author and do not reflect the official policy or position of the Department of Defense or the U.S. Government.

12a. DISTRIBUTION / AVAILABILITY STATEMENT Approved for public release; distribution is unlimited.	**12b. DISTRIBUTION CODE**

13. ABSTRACT *(maximum 200 words)*

The feasibility of a new manufacturing process of ceramic materials in which net shaped products are produced via sintering and simultaneously deforming is studied. A suitable model system of SiO_2-B_2O_3 is chosen due to its desirable properties for liquid phase sintering and its ability to be tested under atmospheric conditions. Samples of compacted powder are prepared and characterized via x-ray diffraction and scanning electron microscopy. Tests to determine the ability of the system to undergo Liquid Phase Sintering are studied. Deformation of samples in compression with concomitant Liquid Phase Sintering at nominally constant true strain rates is performed, and the effects of the amount of liquid phase are investigated. Problems associated with the Liquid Phase Sinter Forming process are identified, and recommendations are suggested for future studies.

14. SUBJECT TERMS Liquid Phase Sintering, SiO_2, B_2O_3, silica, silicon dioxide, boron oxide, deformation, superplasticity, ceramic, powder processing, deformation in presence of a liquid phase	**15. NUMBER OF PAGES** 86
	16. PRICE CODE

17. SECURITY CLASSIFICATION OF REPORT Unclassified	**18. SECURITY CLASSIFICATION OF THIS PAGE** Unclassified	**19. SECURITY CLASSIFICATION OF ABSTRACT** Unclassified	**20. LIMITATION OF ABSTRACT** UL

NSN 7540-01-280-5500

Standard Form 298 (Rev. 2-89)
Prescribed by ANSI Std.

Approved for public release; distribution is unlimited

A FEASIBILITY STUDY OF LIQUID PHASE SINTER FORMING OF A MODEL CERAMIC SYSTEM

Roland Charles Roeder
Lieutenant, United States Navy
B.S. Nuclear Engineering, Purdue University, 1990

Submitted in partial fulfillment of the
requirements for the degree of

MASTER OF SCIENCE IN MECHANICAL ENGINEERING

from the

NAVAL POSTGRADUATE SCHOOL
March 1999

Author: ______________________________
Roland Charles Roeder

Approved by: ______________________________
Indranath Dutta, Thesis Co-Advisor

____
Ashok Gopinath, Thesis Co-Advisor

____
Terry R. McNelley, Chairman
Department of Mechanical Engineering

ABSTRACT

The feasibility of a new manufacturing process of ceramic materials in which net shaped products are produced via sintering and simultaneously deformed is studied. A suitable model system of SiO_2-B_2O_3 is chosen due to its desirable properties for liquid phase sintering and its ability to be tested under atmospheric conditions. Samples of compacted powder are prepared and characterized via x-ray diffraction and scanning electron microscopy. Tests to determine the ability of the system to undergo Liquid Phase Sintering are studied. Deformation of samples in compression with concomitant Liquid Phase Sintering at nominally constant true strain rates is performed, and the effects of the amount of liquid phase present are investigated. Problems associated with the Liquid Phase Sinter Forming process are identified, and recommendations are suggested for future studies.

TABLE OF CONTENTS

I. INTRODUCTION 1
II. BACKGROUND 7
  A. PROCESSING CERAMIC POWDERS 7
    1. Powder Selection 7
    2. Powder Processing 8
    3. Preconsolidation 11
    4. Consolidation 12
  B. LIQUID PHASE SINTERING 17
    1. Rearrangement 18
    2. Intermediate or Solution Reprecipitation Stage 18
    3. Solid State Sintering 21
    4. Effect of Sintering Parameters on Final Density 21
  C. SUPERPLASTICITY 23
    1. Strain Rate Sensitivity of Superplastic Materials 25
    2. Experimental Observations of Superplasticity 26
    3. Mechanisms of Superplasticity 27
    4. Contribution of Grain Boundary Sliding to Total Strain 30
  D. SUPERPLASTICITY OF CERAMICS 31
  E. DEFORMATION IN THE PRESENCE OF A LIQUID PHASE 32
  F. PROPOSED PROCESS WINDOW FOR FORMING CERAMICS DURING LPS 33
III. OBJECTIVES OF THE PRESENT STUDY 35
IV. EXPERIMENTAL METHODS 37
  A. SELECTION OF A MODEL SYSTEM 37
  B. EXPERIMENTAL 41
    1. Powder Processing 41
    2. Liquid Phase Sintering 43
    3. Deformation of Liquid Phase Sintered Compacts 44
    4. X-Ray Diffraction 47
    5. Scanning Electron Microscopy 47
V. RESULTS AND DISCUSSION 49
  A. POWDER PROCESSING AND SHAPE FORMING 49
  B. SINTERING 53
    1. Density Measurements of Sintered Compacts 53
    2. X-Ray Diffraction of Sintered Compacts 57
    3. Scanning Electron Microscopy of Sintered Compacts 59
  C. DEFORMATION OF THE SINTERED COMPACT 67
VI. CONCLUSIONS AND RECOMMENDATIONS 71
LIST OF REFERENCES 73
INITIAL DISTRIBUTION LIST 77

I. INTRODUCTION

Ceramics is both the art and science of making and using solid articles which have as their essential component and are composed mostly of inorganic nonmetallic materials [Ref. 1]. Ceramics have been studied through the ages to improve existing products and develop new and better uses and to improve existing methods of manufacture. The origins of ceramic study are as ancient as the Greek word "keramos" for pottery or earthenware [Ref. 1]. Through most of the historical development of ceramics it was known that ceramics were brittle and experienced fracture with little or no prior deformation. Ceramics possess high melting temperatures, are generally poor conductors of heat and electricity and can be bonded ionically and/or covalently to other compounds [Ref. 2]. It is these properties that have been the driving force in the development of ceramics.

In modern times the study of ceramics has been integrated into almost every scientific field and industry. The importance of ceramics today cannot be underestimated. The nuclear power industry uses uranium-oxide fuels. The machine-tool industry uses alumina ceramics for cutting. Other examples include the glass industry and special electrical and magnetic ceramics for computers and electronic devices [Ref. 1]. Due to the ever increasing usefulness of ceramics, the study of their properties and manufacturing processes becomes even more important.

Ceramic products are inherently brittle and cannot be shaped by normal deformation processes as metallic products can. Basically, two processing methods have been developed for making and forming ceramics for specific products and uses. The first method has been to use fine ceramic particles mixed with a binder that permit shaping (ie. a mixture of clay and water) and heat treatment (firing) to form a cohesive and useful product. However, this method is not practical for all products. A second method involves melting a material to form a viscous liquid and then to shape the material (ie. glasses) during cooling and solidification [Ref. 1]. Both methods have been used to produce effective and useful products.

Powder metallurgy, the method and process of forming specific products for specific complex applications, appeared between the years 1750 and 1850 [Ref. 3]. In the metals' industry, wrought platinum was in demand. The furnaces and refractories of the time were not capable of melting pure platinum, therefore, platinum powder was pressed into compacts, sintered, and hot forged into desired shapes. Eventually refractories and furnaces were developed that could melt platinum and cheaper methods were developed to form wrought platinum. Today, complex metallic shapes can be produced using current "wrought" manufacturing processes. However, the cost of producing a part in a given shape to required tolerances by powder metallurgy may be lower than by "wrought" methods [Ref. 3]. The first commercial application of powder metallurgy occurred when carbon, and later tungsten, was used for incandescent lamp filaments from 1878 to 1898 [Ref. 4]. The part produced by powder metallurgy will still have similar mechanical properties but it will have a lower production cost. The lower cost, rather than any other factor, is the main reason for developing powder metallurgy methods of production.

Ceramics cannot be processed into desired complex shapes using metallic deformation processes. To shape ceramic parts, expensive post-firing machining is required. Post-firing machining can account for 90% of the cost of a finished product [Ref. 5]. In the last fifty years, extensive effort has been expended in the pursuit of using powder metallurgy to produce ceramic parts in order to avoid expensive post-firing machining. Very high temperature operations involving extrusion, rolling and forging were tried with the object to form and shape ceramic objects during production, thus avoiding post-firing machining. The very high temperatures involved in forming ceramics by thermomechanical processing became impractical [Ref. 6]. The technological limitations in obtaining products with large-scale and sophisticated configurations have compelled research workers to look for new ways of preparing these materials [Ref. 7].

The production of ceramic products involves a series of complex tasks. The ceramic particles must be processed into very small particles and then mixed with binders, plasticizers, lubricants and deflocculents. The powder mixture is then shaped by the process of slip casting or pressing. The process of slip casting is adding the powder to a liquid, creating a suspension of ceramic particles in the liquid (slip), and then casting the resulting slurry into a mold. The process of pressing involves compacting the powder into a compact through the use of a die. From either shaping process, the resulting compact or shape is weakly bonded, possessing a low "green" strength. Firing, or sintering, will increase the strength and other desirable mechanical properties. In the sintering process, the ceramic part is heated to a high temperature where densification occurs, resulting in some shrinkage or warpage of the part. For complex parts, post-fire machining is required.

Sintering of ceramics can occur by either solid state sintering or liquid phase sintering. Solid state sintering occurs at high temperatures (~80% of the melting temperature) and is the process whereby diffusion between adjacent particles occurs to effect densification. Due to the very high melting temperatures of most ceramic materials, this is impractical and not commercially attractive. Liquid Phase Sintering occurs at much lower temperatures and is the process whereby a low melting temperature additive is combined with the powder to be sintered. This additive, a sintering aid, melts at a low temperature, providing a short circuit path of diffusion, resulting in enhanced sintering rates [Ref. 8]. Liquid Phase Sintering is a process that is currently being extensively studied to fully understand its connection to other more advanced processes and is the focus of this thesis.

During liquid phase sintering, a small amount of a liquid phase exists at the grain boundaries providing a short circuit path of diffusion. This allows the process of solution-reprecipitation to occur during Grain Shape Accommodation. During deformation at moderate temperatures, a small amount of liquid phase also exists at the grain boundaries. This allows the same process of solution-reprecipitation to occur, resulting in Grain Boundary Sliding. If these two processes, which occur by the same mechanism, can be combined into one process at moderate temperatures, the cost-prohibitive post-fire machining could be eliminated. The advantages of such a system and the promise it holds for better and more cost-effective means of ceramic production are substantial. The objective of this endeavor is to study the combined phenomena of liquid phase sintering with concomitant deformation in order to investigate a unique approach for the production of ceramic products.

II. BACKGROUND

A. PROCESSING CERAMIC POWDERS

The processing of ceramics permits the manufacture of various shapes and sizes from a fine powder. Ceramics processing occurs in four steps: powder selection, powder processing, preconsolidation and consolidation.

1. Powder Selection

The nature of the starting powder has a major effect on the final properties of a ceramic component. Purity, particle size distribution and reactivity must all be considerations in choosing the right powder [Ref. 2].

The purity of the powder influences high temperature properties such as strength, rupture stress, and oxidation resistance. Impurities can have advantageous or detrimental effects. An advantageous effect is when the impurity can form a liquid or glassy phase at a grain boundary at a moderately low temperature [Ref. 9]. This will enhance the solution-reprecipitation mechanism in Grain Boundary Sliding. A detrimental effect is when the impurities are present as inclusions. The inclusions do not appreciably affect properties such as creep or oxidation, but do act as flaws that can concentrate stress and decrease tensile strength [Ref. 2].

The particle size distribution is another important consideration. The particle sizes must be in a range of sizes that permit the maximum packing of particles per unit volume. The ideal starting material to fabricate a fine-grained, high strength ceramic is a small-sized (0.1 to 1.0 μm), equiaxed powder with a narrow size distribution [Ref. 10]. This powder is then capable of being fabricated into dense, uniform green bodies with acceptable handling characteristics.

The final important consideration is reactivity. The change in free surface energy is the major driving force for densification of a compacted powder. Small particles (1 μm or less) have a relatively high surface area with a high free surface energy. There exists a strong thermodynamic drive to decrease their surface area by bonding together. The finer the powder and the greater its surface area, the lower are the temperature and time at temperature for densification [Ref. 2]. These small particles can be compacted and sintered at high temperatures to near theoretical density.

2. Powder Processing

There are generally two methods of processing powders to obtain the desired particle size and size distribution. The particle size and size distribution will determine final properties such as strength and will also determine the amount of porosity. Often purchased powders do not have the desired size or size distribution and must be processed to achieve the desired properties. The two methods of processing are mechanical sizing and chemical sizing.

Mechanical sizing is a general term encompassing many procedures and techniques. Some of the common types of mechanical sizing are elutriation, ball milling, attrition milling, vibratory milling, fluid energy milling, hammer milling and roll crushing [Ref. 4]. Since each technique has been developed for specific applications and size distributions, only ball milling, which is one of the most common types, will be discussed.

Milling in a ball in an effective method for making powders out of brittle materials [Ref. 11]. Ball milling consists of pacing the particles to be ground (the "charge") in a closed cylindrical container with grinding media and rotating the cylinder horizontally so that the media cascade [Ref. 2]. This is shown in Figure 2.1. The rate of milling is determined by the hardness of the media and the particles, the relative size and specific gravity. High specific gravity media can accomplish a specified size reduction much more quickly that low specific gravity media. To reduce the size of large or hard particles will require longer grinding times than small or softer particles.

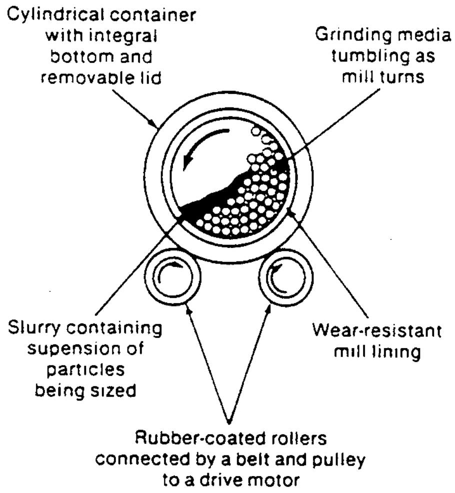
Cylindrical container with integral bottom and removable lid
Grinding media tumbling as mill turns
Slurry containing supension of particles being sized
Wear-resistant mill lining
Rubber-coated rollers connected by a belt and pulley to a drive motor

Figure 2.1. Schematic cross section showing key elements in a ball mill (After Ref. 2).

Ball milling can be conducted wet or dry. Wet milling is illustrated in Figure 2.1 where a liquid is used to create a particle suspension. This will keep the powder particles free flowing and will ensure uniform milling of the particles. Dry milling is conducted without the liquid. This method is difficult because the powder can accumulate in the corners of the mill and avoid milling. This will result in not achieving the desired size and a poor size distribution. The addition of a lubricant can minimize the accumulation of the powder in the corners of the mill. Dry milling has the advantage of not having to remove the liquid through boiling or evaporation from the powder particles after milling. Wet milling results in a powder that has a smaller particle size with a narrow particle size distribution [Ref. 2].

Ball milling has the potential to contaminate the powder being milled. As the particles are being reduced in size, the mill walls and grinding media are also wearing. Contamination can be controlled through the careful selection of the mill lining and the media.

Chemical sizing also involves many processes and techniques depending on the application. Some of the processes are precipitation, freeze drying, hot kerosene drying, Sol-Gel, spray roasting, laser and plasma [Ref. 2]. Chemical sizing techniques have the disadvantages of the pickup of contamination and the control of the particle size distribution.

No matter which process was used to size the particles and to achieve the desired size distribution, the final step in powder processing is screening the powder. Screening is a sorting method of particle sizing. Particles can be separated into size ranges where particles larger than the screen opening remain on the screen and smaller particles pass through the screen. Thus, screening can result in particles with a specific size distribution. Screen sizes are classified according to the number of openings per linear inch and are referred to as mesh sizes [Ref. 4]. A 16-mesh screen has 16 equally spaced openings per linear inch.

3. Preconsolidation

The sized powder is to be formed into the desired shape by pressing or slip casting and then densified. A uniform particle compact will result in a final product with uniform properties and no distortion. In order to achieve this, several additives must be mixed with the powder. The combined effects of the additives are to allow particles to slide past one another to arrange in the closest possible packing and to minimize friction to allow all regions of the compact to experience equivalent pressure. The additives are classified according to function (ie. binder, lubricant, and sintering aid).

The binder is added to increase "green" (unfired) body strength for handling purposes. Binders can be selected based on amount of green strength required, ease of machining, compatibility with the ceramic powder, and the nature of the consolidation process [Ref. 2]. Typical examples of binders are Polyvinyl alcohol (PVA), waxes, rubbers, gelatins and acrylics.

Lubricants are added to decrease particle-particle friction and particle-die wall friction during compaction. They also aid in providing lubrication during die ejection. The amount of lubricant added is typically 0.5 to 1.0 wt % [Ref. 3]. By adding the right amount of lubricant, the compaction process will result in a dense compact with minimal porosity.

Sintering aids are added to aid densification. A glassy phase created by the addition of a small amount of a low melting temperature ceramic greatly enhances densification.

The glassy phase is the means by which Grain Shape Accommodation occurs to reduce porosity and achieve desired densification [Ref. 8].

4. Consolidation

With the powder properly sized, the desired size distribution achieved and with the right mixture of additives, the powder mixture is ready for consolidation. In this step a green shape will be formed. Methods of forming include slip casting, powder pressing and plastic forming [Ref. 2]. Only the method of powder pressing will be discussed here.

The object of powder pressing is to quickly and reproducibly form a nominally defect-free, homogeneously dense powder compact to net shape. The pressing pressure should be high enough to impart sufficient strength for subsequent handling but low enough to avoid excessive wear on the press and tooling [Ref. 12]. Powder pressing involves the compaction of powder in a rigid die by applying pressure along a single axial direction through a rigid punch. A typical pressing operation has three steps: (1) filling the die with powder, (2) compacting the powder to a specific size and shape, and (3) ejecting the compact from the die [Ref. 5].

Die filling influences compaction density, which ultimately determines the size, shape, microstructure and properties of the final sintered product. To optimize die filling and packing uniformity, free-flowing powders are used [Ref 5]. The die should be filled as evenly as possible with the powder. During compaction, pressure is applied and results in densification via particle rearrangement and deformation. The porosity and volume of the compact decrease as the pressure increases, while the coordination number of the particles and compact strength increase. When compaction is completed, the compact must be ejected from the die. The punch used for compression is used to push the compact out of the die. During the compaction and ejection steps, friction is a potentially serious factor to consider.

Friction between particles and the die wall decrease the compaction pressure available as the distance into the compact increases. Uniaxial applied pressure to a compact will be dissipated via frictional forces as the distance into the compact increases. Die wall frictional forces are the primary source of stress gradients that arise during compaction to produce density gradients [Ref. 12]. Compact density is directly related to forming pressure and a forming pressure gradient becomes a density gradient in the compact [Ref. 5]. The density gradients can produce high and low density areas within a compact that densify differently during sintering. High density regions with a higher coordination number will density faster than low density areas, which can lead to defects. As shown in Figure 2.2, the density variations increase as the aspect ratio increases. Friction can be minimized through the use of lubricants on the internal die surfaces, using low aspect ratio compacts or by using isostatic pressing. This will minimize the number of potential defects in the sintered part.

Compaction not only forms the green shape but it also removes porosity as the green shape becomes more dense. The amount of porosity will greatly influence the mechanical properties of the sintered product. Recent studies have shown that cyclic compaction yields higher densities and rupture strengths in sintered compacts than in compacts formed during a single compaction cycle [Refs. 13 and 14]. Cyclic compaction

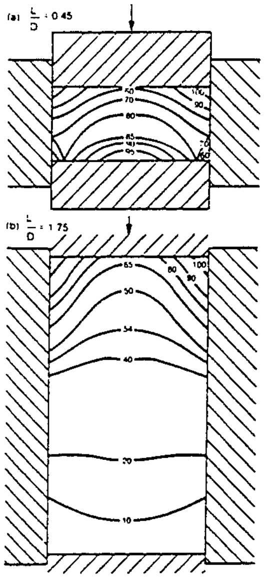

Figure 2.2. Schematic showing density variations in typical powder compacts due to die-wall friction and particle-particle friction (After Ref. 2).

can substantially reduce the remaining porosity in a compact, with results varying from system to system.

Pressing problems are often related to the characteristics and properties of the powder. This includes how the powder flows into and fills the forming die, how the powder deforms under the pressing pressure, how uniformly the applied pressure is transmitted through the compact during forming and the amount of stored elastic-strain energy released upon ejecting the compact from the die [Ref. 12]. The release of the elastic-strain energy is characterized as springback. Springback is the expansion of the compact upon ejection from the die in a direction perpendicular to the pressing direction. This occurs as a result of the residual stresses in the compact after die ejection. Excessive springback can produce catastrophic flaws within the compact. Limiting the compaction ratio below a threshold value minimized effects of springback [Ref..5]. Some common defects that are indicative of springback are end capping, ring capping, laminations and vertical cracks as shown in Figure 2.3.

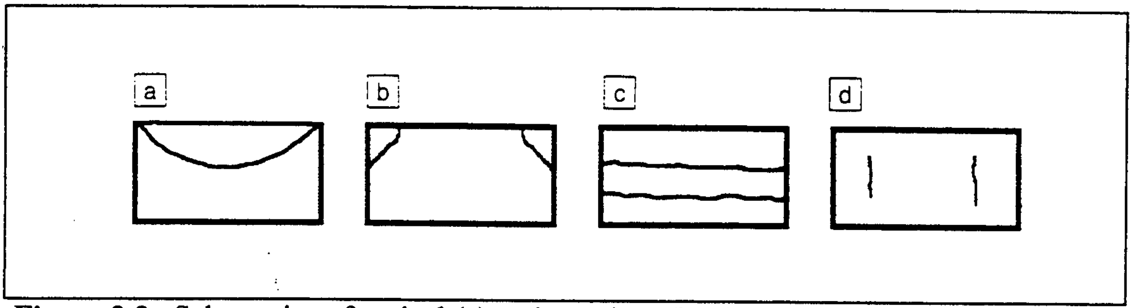

Figure 2.3. Schematics of typical (a) end capping, (b) ring capping, (c) laminations and (d) vertical crack defects in cross sections of cylindrical powder compacts pressed uniaxially from the top down (After Ref. 5).

End capping is a central cone-shaped separation that forms at the pressing punch face. It is common in bodies having poor green strength and high springback. High die wall friction and high pressing pressure contribute to the production of this defect [Ref. 12]. It is caused during ejection from the die. As the top part of the compact clears the die, it rebounds to a larger cross section while the remaining part of the compact is restrained by the die walls. A tensile stress develops just above where the compact clears the die. Minimizing die wall friction minimizes end capping effects [Ref. 2].

Ring capping is an outer-ring separation that forms at the outer edge of the pressing punch face. It is caused by poorly machined tolerances between the punch and die. It is minimized by improved tolerances.

Laminations are periodic circumferential cracks that originate on the die surface perpendicular to the pressing direction. As a compact is being ejected from a die, the material already ejected will rebound to a larger cross section and the material still in the die is constrained by the die walls. This places a tensile stress in the material just above the top of the die and can result in a series of cracks when die wall friction is high. Laminations are minimized by reducing die wall friction.

Vertical cracks are elongated cracks that form parallel to the pressing direction in the exterior region of a compact. These defects occur in high aspect ratio compacts.

As a result of consolidation, a "green" compact is formed that has "green" properties. The properties of green compacts are routinely measured to determine if any flaws exist [Ref. 11]. One of the properties that is checked is the density of the compacts. This is determined by the immersion-density technique (ie. Archimedes' method) shown in Figure 2.4.

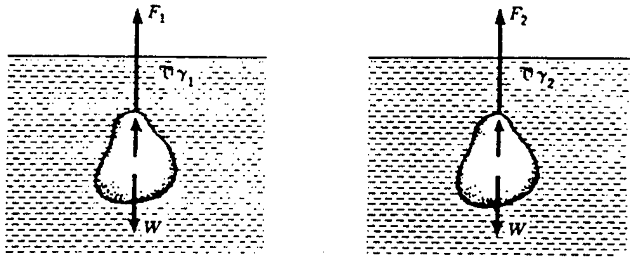

Figure 2.4. Free-body diagrams of a body suspended in fluids of different specific gravity (From Ref. 15).

Archimedes' method involves the simple application of the laws of buoyancy. First, a body is suspended in a liquid of specific gravity γ_1 and the force F_1 is measured. Then, the body is immersed in a fluid of specific gravity γ_2 and the force F_2 is measured. The equations of static equilibrium are:

$$F_1 + V\gamma_1 = W \qquad\qquad F_2 + V\gamma_2 = W \tag{1}$$

These equations are solved simultaneously yielding:

$$W = \frac{F_1\gamma_1 - F_2\gamma_2}{\gamma_2 - \gamma_1} \qquad\qquad V = \frac{F_1 - F_2}{\gamma_2 - \gamma_1} \tag{2}$$

The density of a compact is calculated as $\rho = \boldsymbol{W/\mathrm{g}V}$.

B. LIQUID PHASE SINTERING

Sintering is a process in which the compact is heated to a temperature below its melting point in a controlled atmosphere to allow densification to occur. When the temperature is raised to a temperature sufficient for one of the constituents to melt and a solid/liquid interface is formed with the other constituents, the process is known as Liquid Phase Sintering (LPS). The rate of sintering is greatly enhanced by the presence of a liquid phase [Ref. 1].

There are basically two types of liquid phase sintering [Refs. 2, 3 and 8]. In type 1 LPS, the liquid is present during the entire process while at the sintering temperature between the solid and liquid components. In type 2 LPS, often referred to as "transient liquid phase sintering," the liquid forms when the compact is heated to the sintering temperature, but disappears via diffusion into the solid or is carried away through evaporation [Refs. 3 and 8]. Type I LPS is a densification and growth process that occurs in three stages.

1. Rearrangement

As the compact is heated, solid state sintering occurs and is driven by the chemical concentration gradient in the microstructure [Ref. 8]. Upon heating to the eutectic temperature and the formation of a liquid phase, there is a rapid rearrangement of particles that increase the density of the compact. The amount of liquid present determines the extent of densification. For large amounts of liquid present, nearly full densification can be achieved. For small amounts of liquid, a rigid solid skeleton can form inhibiting densification. Densification occurs due to the capillary force exerted by the liquid on the solid particles. Capillary action allows the liquid phase to fill the interstices, with the smaller capillaries being filled first and larger capillaries next, depending on the availability of the liquid. Simultaneously, the solid particles rotate and rearrange to pack together to a higher density. At the conclusion of this stage, there is still considerable porosity present. The elimination of porosity continually increases the compact's viscosity resulting in the densification rate to continuously decrease during this stage [Ref. 8].

2. Intermediate or Solution Reprecipitation Stage

Solubility and diffusivity effects become dominant when continued particle rearrangement is no longer feasible. Continued densification and grain growth occur by the process of dissolution of the solid phase in the liquid and reprecipitation on existing grains.

Densification during this stage requires solid solubility in the liquid phase and is dependent on mass transfer through the liquid. The porosity decreases with time as microstructural changes lower the system energy by the elimination of interfacial area. This is known as Grain Shape Accommodation and is shown in Figure 2.5. The solution-reprecipitation mechanism allows the solid spherical grains to change shape to better fill the available space. The adjusted grain shape has a higher solid-liquid surface area than a sphere, but the elimination of pores and the associated surface energy provides for a net energy decrease [Ref. 8]. Grain Shape Accommodation occurs by contact flattening, dissolution of small grains and solid-state diffusion.

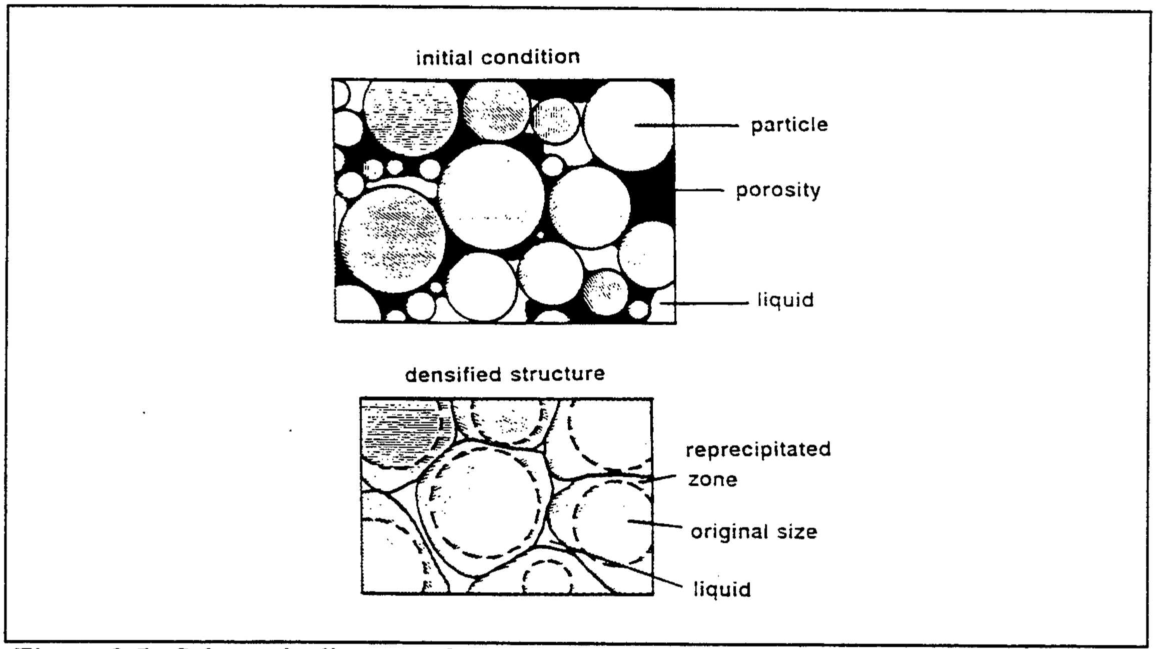

Figure 2.5. Schematic diagram of Grain Shape Accomodation. Densification occurs through the elimination of smaller particles and preferential precipitation on the larger particles via the solution-reprecipitation mass transport mechanism (From Ref. 8).

In contact flattening the wetting liquid causes a capillary force, which induces a stress at the point of grain contact. To relieve the stress, some of the solid dissolves into the liquid at the contact point and precipitates at a region away from the grain contacts. Densification results from the center-to-center motion of neighboring grains. Smaller grains have higher capillary stress and this results in higher rates of contact flattening. The material transport away from the contact point determines the densification rate. As the size of the contact zone grows, the stress induced in the contact region (σ=F/A) along the interface decreases and densification slows.

The dissolution of fine grains is dependent on the grain size distribution. Small particles have a larger free surface energy than large particles and are more likely to dissolve into the liquid phase. This solubility difference creates a concentration gradient in the liquid. The small particles dissolve into the liquid and are transported to and reprecipitate on the larger particles. This process is call Ostwald Ripening [Ref. 8]. Thus, the large grains grow and undergo shape change accommodation at the expense of neighboring small grains. This results in decreased porosity.

Solid state diffusion relies on diffusion through the solid and upon contact flattening. This mechanism is generally not important because the rates of diffusion through the liquid are higher than through the solid, except where solubility of the solid in the liquid is low [Ref. 8].

At the beginning of the intermediate stage, contact flattening is the predominant mechanism of continued densification. This is due to the initial contact stresses being extremely large as the result of point contacts between adjacent spherical particles. As the rate of densification by contact flattening decreases due to increased contact surface area, the mechanism of solution-reprecipitation will dominate [Ref. 8].

3. Solid State Sintering

Complete densification can be achieved during stages one and two of liquid phase sintering. However, in some cases, a rigid solid skeleton will have formed which inhibited complete densification. In these cases, further densification can only be achieved by solid state sintering. Densification during this stage is slow when compared to the first two stages. Holding the compact at temperature to effect solid state sintering can result in excessive grain coarsening and degeneration of the compact's material properties [Ref. 3]. This mechanism is also operative during the first two stages but only dominates once the first two stages have occurred.

4. Effect of Sintering Parameters on Final Density

Generally there are only a few controllable parameters that can affect the final sintered density of a compact. These parameters are the particle size, the solubility of the solid phase in the liquid, the distribution of the liquid phase, the sintering temperature, the time at the sintering temperature and the sintering atmosphere. By adjusting these parameters, the final porosity, the final skeletal microstructure and the final grain size can be controlled, which ultimately control the final density of the compact [Ref. 8].

The particle size should be small. Smaller particles result in higher capillary pressure and also have higher surface energies. Thus, there is a higher driving energy for densification [Ref. 2]. By starting with a small particle size, higher densities are easier to achieve.

The solubility of the solid phase in the liquid is dependent on the system and the temperature. From the system equilibrium phase diagram, one can determine the range of temperatures where the solid phase will have solubility in the liquid phase. As long as there is adequate solubility, liquid phase sintering will occur and will result in higher densities than if no liquid phase were present [Ref. 8].

The distribution of the liquid phase prior to melting can be critical to the final density. The liquid phase should be homogeneously distributed throughout the compact. This ensures that there will be a sufficient amount of the liquid phase throughout the compact to support solution-reprecipitation. In regions where there may be inadequate amounts of liquid phase present, solid state sintering will occur, forming a rigid solid skeleton which inhibits further densification. Thorough mixing of the powder will ensure a homogeneously mixed liquid phase [Ref. 8].

The sintering temperature is also a most important parameter on final density. Generally, the sintering temperature should be high enough to support a liquid phase, but low enough to prevent excessive grain growth and premature solid state sintering. Other temperature dependent effects that must be considered in choosing the sintering temperature are surface tension, liquid viscosity, diffusivity and solid solubility in the liquid phase. Higher temperatures usually favor liquid phase sintering [Ref. 8]. Higher temperatures reduce surface tension forces and liquid viscosity, while increasing diffusivity and solid solubility in the liquid phase. Thus, higher temperatures usually result in higher density compacts. Excessively high temperatures are to be avoided as they promote grain growth and solid state sintering.

The time at the sintering temperature is another controllable parameter of the sintering process. The time should be sufficient for particle rearrangement and solution-reprecipitation to occur without excessive coarsening of the grains. As the time at the sintering temperature is increased, the final density will increase. Thus there is an optimum time to achieve a high final density while maintaining a small grain size [Ref. 8].

The last controllable parameter is the atmosphere in which the sintering will occur. A flow of gases is needed for purification and sintering in the furnace [Ref. 16]. The gaseous products must be continuously removed from the furnace to effect the continuous removal of gaseous products from the compact. As the gaseous products are removed, the porosity decreases and the final density increases.

C. SUPERPLASTICITY

Superplasticity is the ability of a polycrystalline material to exhibit, in a generally isotropic manner, very high tensile elongations prior to failure [Ref. 17]. The first detailed investigation of the superplastic effect in metals is generally attributed to C. E. Pearson in 1934, when an elongation of 1950% was achieved in an aged Bi-44% Sn eutectic alloy [Ref. 18]. The first clear demonstration of superplastic behavior in a ceramic material occurred in 1986 when F. Wakai and co-workers reported tensile elongations of over 100% in a yttria-stabilized tetragonal zirconia [Ref. 18]. It is recognized that the superplastic process has many potential applications in the ceramic forming industry and the potential utilization of ceramic materials as components in high temperature application [Ref. 18]. The development of high strain rate superplasticity is expected to have a significant technological impact on the commercial applications of superplastic materials, since an increase in forming rate will result in a great reduction in forming time [Ref. 19].

Generally, there are two basic types of superplasticity, termed transformation and structural superplasticity [Ref. 18]. Transformation superplasticity refers to temperature cycling through a phase change, where internal stresses generated aid a small externally applied stress and cause the material to behave superplastically [Refs. 18 and 20]. Structural superplasticity refers to attaining superplastic elongations at constant temperatures without a phase change. Both types superplasticity may be important in selected ceramics under certain conditions, but technological requirements dictate major emphasis on the development of ceramics capable of exhibiting structural superplasticity [Ref. 18].

Microstructure is an important criterion to indicate the potential for superplastic deformation in ceramics. A fine grained (<1 μm, typically 0.3 to 0.5 μm) equiaxed microstructure that is stable at high temperatures and resistant to grain growth is required [Ref. 21]. Fine grain sizes enhance superplastic deformation [Ref. 22]. In materials that have been superplastically deformed, the grains remained equiaxed with little or no significant elongation along the tensile axis. The lack of any change in shape has been taken as direct evidence that grain boundary sliding with accompanying grain rotation and mass transport is the dominant deformation process in superplasticity [Ref. 17].

1. Strain Rate Sensitivity of Superplastic Materials

The flow stress and the true strain rate are related through the expression

$$\sigma = \beta(\dot{\varepsilon})^{m} \qquad \textbf{(3)}$$

where β is a constant which incorporates the dependence on temperature and grain size and m is the strain rate sensitivity (defined as $\partial \ln \sigma / \partial \ln \dot{\varepsilon}$) which is independent of temperature. High values of m ($m \geq 0.3$) are required for superplasticity [Ref. 17]. The strain rate sensitivity is determined experimentally by conducting a series of tests at constant true strain rates. The slope of the true stress versus true strain rate logarithmic plot is the strain rate sensitivity [Ref. 17].

The value of the strain rate sensitivity of a material is directly related to the ability of the material to resist the development of a tensile necking region during a tension test [Ref. 17]. This can be shown theoretically by substituting $\sigma = F/A$ and $\varepsilon = (-1/A)(dA/dt)$ into equation (3). The new equation, after substitution is:

$$\frac{dA}{dT} = -\frac{FA^{m-1/m}}{\beta m} \qquad \textbf{(4)}$$

With this form of the equation the value of the strain rate sensitivity can be bracketed between 0 and 1. A material with a strain rate sensitivity of 0 corresponds to a metal at low temperature. Thus, its flow stress has no dependence on strain rate. A material with a strain rate sensitivity of 1 corresponds to a Newtonian fluid for which the stress and strain rate are linearly related and also exhibits dA/dt = constant, resulting in the reduction in cross-sectional area per unit time being a constant [Ref. 23]. In other words, when a neck forms at a location along the length of a specimen in tension, the neck deforms at the same rate as the material outside the necked region [Ref. 24]. The reduction in the necked area per unit time will be greater than in regions away from the neck for any value of strain rate sensitivity less than 1. Higher values of strain rate sensitivity indicate greater resistance to necking and tensile failure.

2. Experimental Observations of Superplasticity

Figure 2.6 is a plot of the true stress versus true strain rate for a superplastic material. The slope of the curve (m) is the strain rate sensitivity and it can be separated into three distinct regions [Ref. 25]. Regions I (low stress-low strain rate) and region III (high stress-high strain rate) have low strain rate sensitivities (m). Region II is a transition

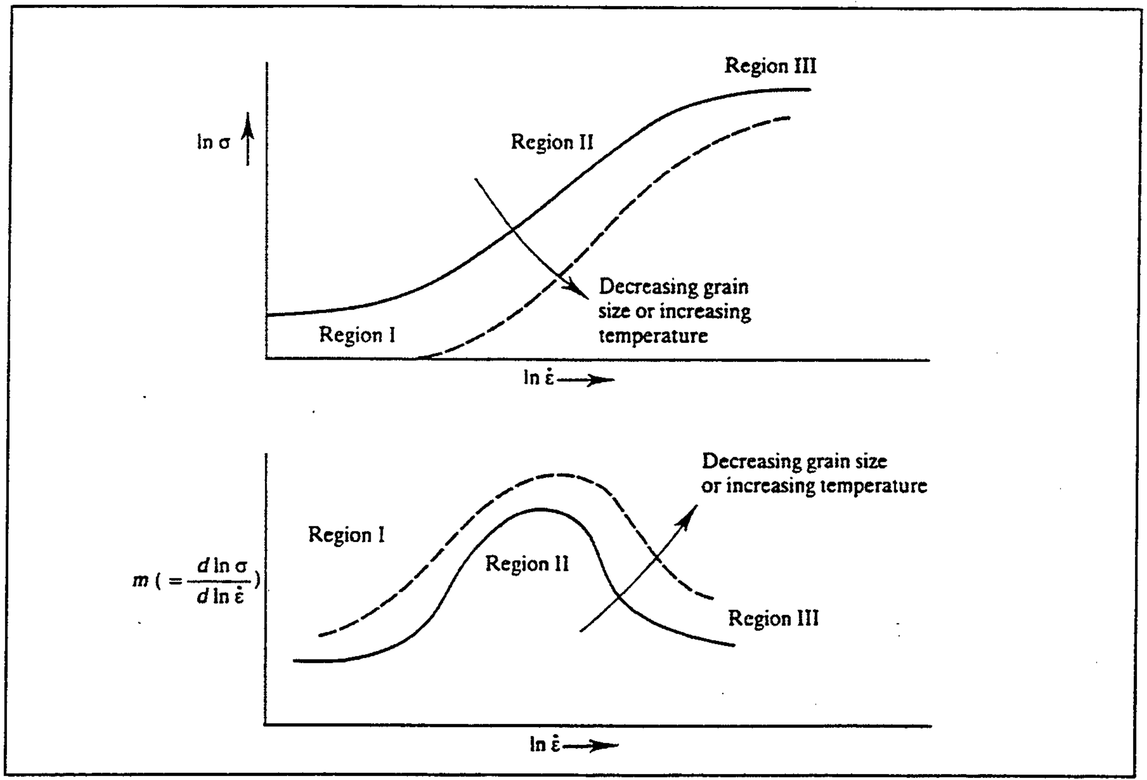

Figure 2.6. Schematic showing sigmoidal shape of the stress-strain rate plot for a superplastic material. The strain rate sensitivity (slope of the curve) is low in regions I and III, but high in the superplastic region II (From Ref. 24)

region and has a high strain rate sensitivity. Superplasticity occurs in region II with strain rate sensitivity (m) values of 0.3 to 0.8 [Ref. 17]. Note that in Figure 2.6 that the plot of the curve can shift due to the dependence of superplastic deformation on grain size and temperature.

3. Mechanisms of Superplasticity

Is is known that the dominant mechanism of superplasticity is grain boundary sliding [Ref. 17]. Many experiments have been conducted to determine the contribution from grain boundary sliding to the total strain and the results generally give contributions lying in the range of about 50-70% [Ref. 26]. Models have been developed to determine the nature of the "missing" strain and are classified by the accommodation mechanisms: diffusional creep, accommodation by dislocation flow, or a combination model of the two [Ref. 21].

Diffusional creep occurs in polycrystals without the presence of a liquid phase [Ref. 27]. Mass transport occurs by vacancy diffusion as described by the Nabarro-Herring and Coble creep mechanisms. In Nabarro-Herring creep, mass transport and vacancy diffusion occurs through the volume of the grains, while in Coble creep, the path of diffusion is along the grain boundaries. The creation and annihilation of vacancies occur by climb at the boundaries.

Dislocation flow occurs by solution-precipitation when a liquid phase is present at the grain boundaries [Ref. 21]. Mass transport occurs through diffusion in the liquid phase. When an atom reaches a boundary step, the step moves along the surface of the grain. The solution-precipitation of an atom occurs by movement of the step. This assumes that a thin continuous liquid film is able to support stress to some extent [Ref. 21]. The rate of dislocation flow in controlled by the viscosity of the intergranular liquid phase, the solubility of the solid phase in the liquid, the formation energy of the surface step and the structure of the adsorption layer on the grain surface [Ref. 21].

A combination model involves both the creation and annihilation of vacancies and the detachment and reattachment of atoms. This model combines the previous two models to account for all mass transport.

A model proposed by Ashby and Verral includes a grain-switching event that provides for material deformation and the preservation of the grain shape [Ref. 28]. Figure 2.7 demonstrates the grain-switching mechanism. In the initial state, a stress is applied to the four grains as shown. The applied stress results in lower activation energies for vacancy formation in the top and bottom of the grains. This results in a vacancy concentration gradient and a flow of vacancies. Opposite to the flow of vacancies is the mass flow in the direction of the applied stress. Mass flow can occur through the grain interior or along the grain boundaries.

In the intermediate state of grain-switching, there is an increase in the grain-boundary surface area due to the net mass flow. The increased grain boundary surface area requires energy and represents a "threshold stress" below which the grain-switching mechanism cannot occur [Ref. 24]. When the threshold stress is exceeded, some irreversible work is performed by the applied stress to overcome the increase in surface area before the diffusional flow and grain-switching mechanisms can occur. This results in a reduction the grain boundary surface area and results in the preservation of the grain shapes in the final state. The strain rate for the grain-switching mechanism greatly exceeds the rate for conventional creep mechanisms due to the fact that only about 1/7 of the volumetric flow of mass is required as compared to diffusional creep [Ref. 24].

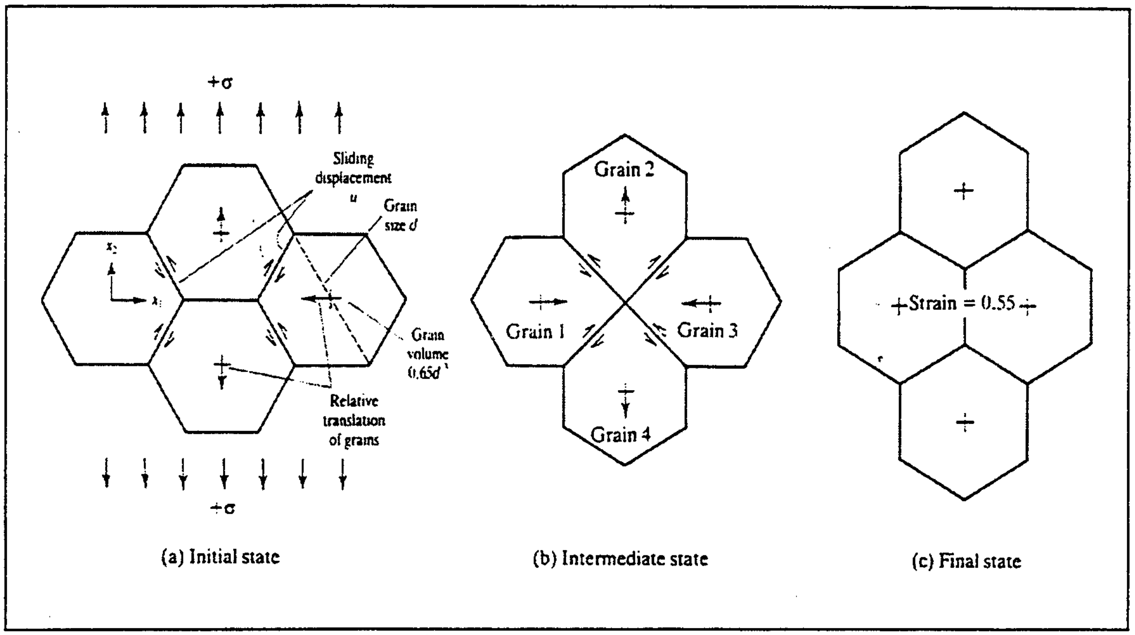
+σ
Sliding displacement u
Grain size d
x_2
x_1
Grain volume $0.65d^3$
Relative translation of grains
+σ
Grain 2
Grain 1
Grain 3
Grain 4
Strain = 0.55

(a) Initial state (b) Intermediate state (c) Final state

Figure 2.7. Schematic showing the grain-switching mechanism proposed by Ashby and Verral. Note that a true tensile strain of 0.55 occurs as a result of grain-switching (From Ref. 24).

As proposed by Ashby and Verral, grain-switching creep occurs on a competitive process with dislocation creep. The grain-switching mechanism dominates in region I and the dislocation creep dominates in region III. In the superplastic region II, both grain-switching creep and dislocation creep occur. In region I, the low strain rate sensitivity has been associated with the presence of impurities in superplastic allows [Ref. 17]. Impurities at the grain boundaries inhibit grain boundary sliding at low stress levels and lower the achievable strain rates dramatically. Careful experiments by

Mohamed *et. al.* have shown that it is possible to eliminate region I in a Zn-22% Al eutectoid alloy, so that region II extends over several orders of magnitude of stain rate, by using a super-pure (99.999%) alloy [Ref. 29].

4. Contribution of Grain Boundary Sliding to Total Strain

Several investigations have attempted to determine the nature of the "missing" strain in superplastic materials. Two possibilities have been proposed: the strain may be due to diffusion creep acting concurrently with superplastic flow or the strain may be due to the movement of intragranular dislocations [Ref. 26].

An examination of the experimental evidence leads to the conclusion that there is no significant strain as a result of diffusional creep in superplastic materials. Diffusion creep would be evidenced by the elongation of individual grains and this is contrary to many well-documented experimental observations that the grains remain essentially equiaxed after superplastic deformation [Ref. 26].

It is usually assumed that the "missing" strain is due to the movement of dislocations within the grains. However, experiments on a superplastic Pb-62wt%Sn eutectic alloy, at elongations up to 800%, have shown that the movement of intragranular dislocations occurs only as an accommodation process for grain boundary sliding and that the net contribution to the total strain is close to zero [Ref. 30].

An examination of the experimental methods used to measure grain boundary sliding was conducted by Langdon [Ref. 26]. He showed that the contribution of grain boundary sliding to the total strain ε gives values in the range of 50-70% for superplastic materials. Thus, the "missing" strain is 30-50% of the total strain. He concluded that the experimental values are underestimates of the true values of the sliding contributions because of limitations in the measuring procedures and there is no "missing" strain. Grain Boundary Sliding accounts for essentially all of the deformation under optimum superplastic conditions.

D. SUPERPLASTICITY OF CERAMICS

Since the 1960s, the field of superplasticity has expanded dramatically as high tensile ductilities in a wide range of materials, including ceramics, have been achieved. The first genuine demonstration of superplasticity in a ceramic was announced on July 5, 1985 by Wakai et. al. [Ref. 17]. They demonstrated superplasticity in a yttria-stabilized tetragonal zirconia polycrystalline material (3Y-TZP) at the Government Industrial Research Institute in Nagoya, Japan [Ref. 18]. Since this breakthrough, superplastic data has been complied on other ceramic systems such as Al_2O_3/Y_2O_3 and Hydroxyapatite [Ref. 17].

Although ceramics are inherently brittle, they have two characteristics which are useful in attaining high superplastic ductilities [Ref. 31]. First, the grain sizes are small and are on the order of the micron and sub-micron range. Second, the grain boundary mobilities are low and this tends to make ceramics resistant to grain growth during superplastic deformation.

Nieh and Wadsworth have shown in recent experiments that the presence of a liquid phase is not required for superplasticity in fine-grain ceramics [Ref. 19]. Although the presence of a liquid phase is not required, it is known that a small amount of liquid phase in a ceramic can change its deformation properties. Raj *et. al.* have shown that a liquid phase at the grain boundaries enhance the grain boundary diffusivity by up to several orders of magnitude and thus, greatly enhance superplastic deformation [Ref. 32].

E. DEFORMATION IN THE PRESENCE OF A LIQUID PHASE

Deformation in the presence of a liquid phase has been utilized for many years. An example is dentists who depend on the interim plasticity of an amalgram in order to properly set fillings in a cavity [Ref. 9]. Sintering and creep involve similar mass transport mechanisms and are greatly accelerated by the presence of a liquid phase Ref. 9].

The amount of liquid phase present will determine the mechanism by which a liquid containing rigid solid particles will deform. A viscous liquid containing solid particles will exhibit large elongations by rheological flow and not by superplasticity [Ref. 21]. Superplasticity is the dominant deformation in ceramics when the volume fraction of the glass phase is less than 10%. For glass phase volume fractions greater than 10%, rheological flow is dominant and is the dominant mechanism [Ref. 21].

Polycrystalline solids with a small amount of liquid phase present at the grain boundaries deform by grain boundary sliding via solution-precipitation creep. The liquid phase acts as a medium for mass transport by allowing solution and reprecipitation of the solid phase [Ref. 21]. Applied tensile stresses are present during forming and the grain boundaries must be able to support tensile loading. For a continuous liquid phase at the boundary, the grain boundary must be able to support a normal tensile stress without cavitating prematurely in order for the material to behave superplastically [Ref. 34]. Clarke showed this assumption to be true when normal deformation stresses were applied to crystals with a small amount of glassy phase present at the grain boundaries. Interatomic forces developed between the solid and liquid layers immediately adjacent to the solid and were suitably oriented to provide a normal load bearing capability [Ref. 35]. Whether or not a material with a liquid phase at the grain boundary will exhibit superplasticity is dependent on both the amount and distribution of the liquid phase. A thin layer of grain boundary liquid with the liquid concentrated primarily in pockets at triple grain junctions is more conducive to superplastic forming due to cavitation resistance at the grain boundaries, which eventually limits tensile ductility [Ref. 36].

F. PROPOSED PROCESS WINDOW FOR FORMING OF CERAMICS DURING LPS

Manufacturing ceramic products with complex shapes and sizes is very expensive due to the post-fire machining process. During manufacture, the ceramic powder is sintered to produce densification and strengthening. A liquid phase at the grain boundary increases the rate of sintering and will lower the required sintering temperature. A solid with a small amount of liquid phase present at the grain boundaries will deform by grain boundary sliding via solution-precipitation creep through the liquid phase.

The goal of the present study is to combine the processes of sintering and liquid phase enhanced deformation to achieve net-shaped products. The sintering process will be allowed to occur without applied stress until the rearrangement stage is completed. In stage II sintering, contact flattening via diffusional flow near stress concentrations will also be allowed to progress. Part way through stage II, before Ostwald ripening has become the dominant deformation mechanism, a stress will be applied. Thus, in stage II of the sintering process, the deformation phase will occur with Ostwald ripening. Deformation will occur via grain boundary sliding by solution-precipitation mass transport in the liquid phase. Finally, the solid state sintering process will be allowed to occur for strengthening of the net-shaped product.

III. OBJECTIVES OF THE PRESENT STUDY

The objective of the current study is to explore the suitability of SiO_2-B_2O_3 as a model system for studying superplastic deformation concurrently with liquid phase sintering with SiO_2 as the solid (high melting temperature) phase and B_2O_3 as the liquid (low melting temperature) phase. This system has the capability to allow processing at relatively low temperatures in air and also possesses the ability of liquid phase sintering and deformation in the presence of a liquid phase. With the combination of these two steps, a net-shaped product can be produced in one manufacturing step. In addition to studying the suitability of the model system for study of liquid phase sintering, a preliminary investigation of the deformation behavior of the SiO_2-B_2O_3 system above its melting point is carried out.

IV. EXPERIMENTAL METHODS

A. SELECTION OF A MODEL SYSTEM

The SiO_2-B_2O_3 system was chosen as the model system for the study of the LPSF process. This system has potential use in the electronics industry as an insulation-layer material [Ref. 10]. As seen in the phase diagram (figure 4.1), B_2O_3 is the low melting temperature component (T_m=450°C) and SiO_2 is the high melting temperature component (T_m=1710°C). In order for the LPSF process to occur, the solution-reprecipitation mechanism must be operative above the melting point of B_2O_3. At 900°C, SiO_2 has a solubility of approximately 65 wt % in liquid B_2O_3, and at 1200°C, SiO_2 has a solubility of approximately 80 wt % in liquid B_2O_3. It is this solubility of SiO_2 in B_2O_3 that allows the solution–reprecipitation mechanism to occur.

At low temperatures, the powder mixture is a combination of SiO_2 particles and 10 wt % of B_2O_3 particles. As the temperature is increased, the concentration of the constituents is expected to remain the same until the melting point of B_2O_3 is reached, since B_2O_3 and SiO_2 have no solid solubility. At this temperature and above, the composition of the liquid phase changes according to the Lever rule as shown on the phase diagram (Figure 4.1). At any temperature above the melting point of B_2O_3, solid SiO_2 is in equilibrium with liquid SiO_2 and B_2O_3 where the liquid composition is given by the line AB. The relative weight fraction of the solid SiO_2 and the liquid with which it is in equilibrium is given by [Ref. 38]:

$$W_{SiO_2} = \frac{C_L - C_o}{C_L - C_{SiO_2}} \qquad (5)$$

$$W_{liquid} = \frac{C_o - C_{SiO_2}}{C_L - C_{SiO_2}} \quad (6)$$

where: C_L = composition of B_2O_3 in wt %.
C_o = composition of the liquid in wt %.
C_{SiO_2} = composition of SiO_2 in wt %.

SiO_2 exists in a number of different polymorphic forms in various temperature ramps. At 573°C, a displacive transformation occurs as low quartz transforms into high quartz [Ref. 1]. This displacive transformation occurs quickly with a volume change of 1.6% [Ref. 2]. Displacive transformations involve a distortion in the structure, such as a change in bond angles, but does not include the breaking of bonds. At 867°C, a reconstructive transformation occurs as high quartz transforms slowly into tridymite. Reconstructive transformations occur when bonds are broken and a new structure is formed. Because of the slow transition of quartz into tridymite, it is likely that the solid phase produced during sintering between 867°C and 1200°C will be a mixture of tridymite and quartz. All of the present experiments were conducted between 900-1200°C. Upon cooling to room temperature, the reverse transformations occur. The reverse transformation from tridymite to quartz occurs slowly. As a result of which a mixture of tridymite and quartz is expected after sintering between 900-1200°C even after cooling to room temperature.

Sintering of the compact and subsequent deformation of the compact were conducted in two separate steps. The first step was sintering the compact to achieve the highest densification possible. The second step was to deform the compact to study the effects of deformation. These steps are described in detail subsequently. In both steps, the mechanism of solution-reprecipitation is the dominant mode of mass transport for Grain Shape Accommodation (which gives rise to sintering) and Grain Boundary Sliding (which produces superplastic deformation).

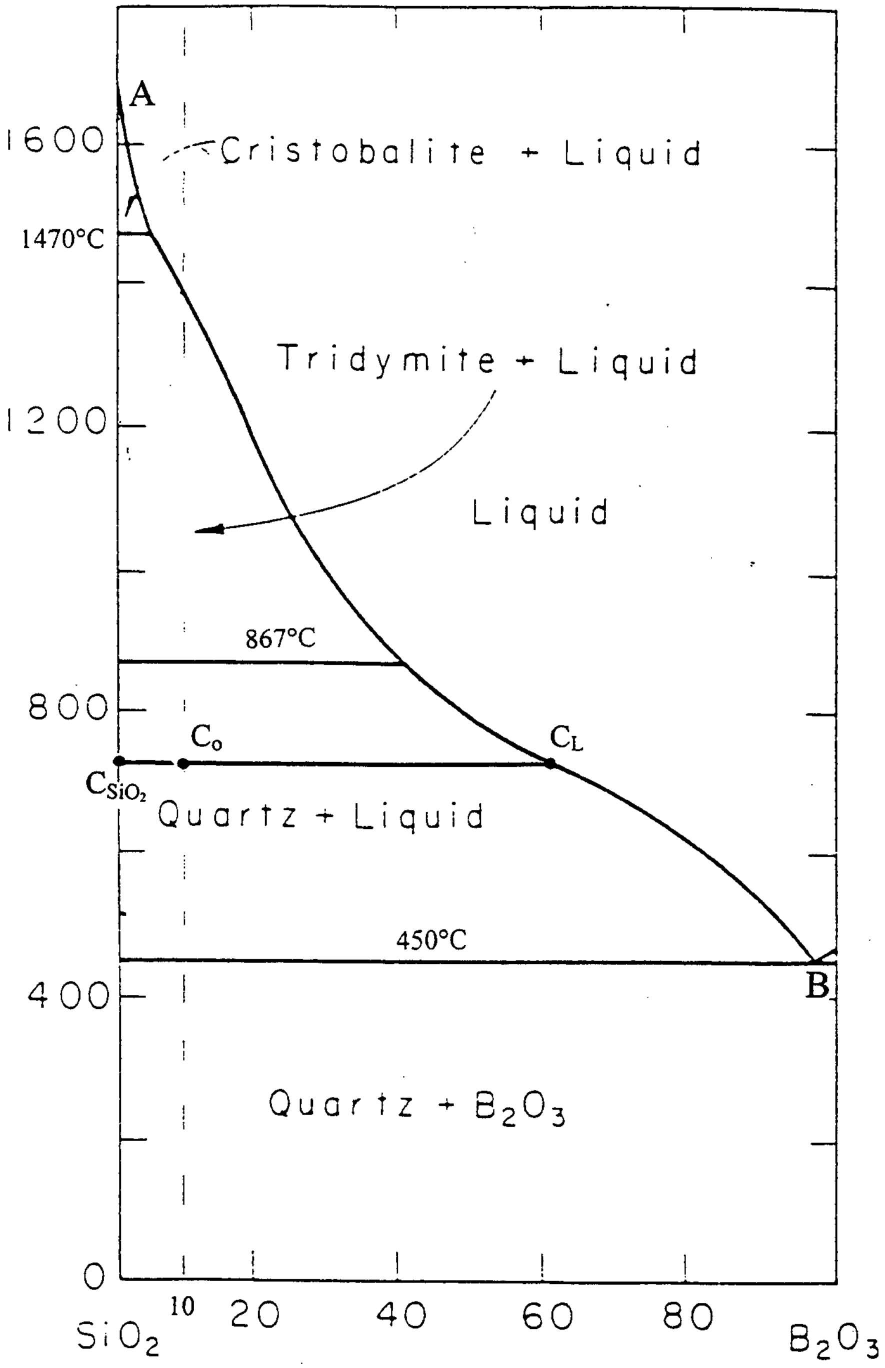

Figure 4.1. Phase diagram for the SiO_2-B_2O_3 system (After Ref. 37).

B. EXPERIMENTAL

1. Powder Processing

Ceramic powder processing usually occurs in four steps. The four steps are selection, preparation, pre-consolidation and consolidation. For the SiO_2-B_2O_3 system, the powder selection step involved purchasing crystalline quartz with a purity of 99.6% and a –325 mesh size. In the preparation step the SiO_2 powder was reduced in size and mixed using an alumina-fortified ball mill with zirconia grinding media. The ball mill was filled to 55% of its total internal volume with the zirconia grinding media prior to powder loading. Due to the hygroscopic nature of the SiO_2-B_2O_3 system, anhydrous cyclohexane (99.5% pure) was used as the fluid medium in the ball mill. The SiO_2 powder was milled in the ball mill with cyclohexane for 72 hours to effect a particle size reduction.

Separately, the B_2O_3 powder was milled with cyclohexane for 24 hours to effect a particle size reduction. The resulting B_2O_3 slurry was then poured into a tray and the cyclohexane evaporated off, with the B_2O_3 powder being stored in a desicator until use.

The pre-consilidation step involved the addition of B_2O_3 and several additives to the sized SiO_2 powder. The binder, lubricant, plasticer and sized B_2O_3 powder were added to the ball mill containing the sized SiO_2 powder. The mixtures used contained SiO_2 with 10 wt % B_2O_3 powder, a binder of 1.0-3.0 wt % polyvinyl alcohol (PVA), a plasticizer of 0.5-3.0 wt % poly-ethylene glycol (PEG) and a lubricant of 0.5-3.0 wt % zinc-stearate. The final mixture was milled for 24 hours for further particle size reduction and to ensure thorough mixing of all of the particles. The resulting slurry was poured into a tray and the cyclohexane evaporated off, with the final mixture stored in a desicator until used in the compaction process.

The final step of ceramic powder processing is consolidation. A cylindrical punch and die was required to compact the powder. The punch and die was fabricated from an A-2 tool steel [Ref. 41]. The A-2 tool steel is an air hardenable, medium-alloy cold-work steel ideal for uses such as a punch and die where close tolerances and a high resistance to wear is required. It is hardenable to HRC 62 with little or no distortion with a very high resistance to cracking. It was machined in accordance with Figure 4.2 and then given a hardening treatment in a Lindberg model 1442 furnace. The hardening treatment consisted of preheating the machined parts to 790°C for 30 minutes and then transferring them to another furnace where they were hardened at 950°C for 30 minutes [Refs. 40 and 41]. The parts were removed from the furnace and allowed to air cool to room temperature. Final hardness was measured to be HRC 60.

The internal punch and die surfaces were coated with a suspension of Molybdenum Di-Sulfide (MoS_2) in methanol to provide for surface lubrication. Following the application of the suspension, the die was allowed to stand at room temperature to allow the methanol to evaporate, leaving a thin layer of MoS_2 on the internal surfaces. The punch and die assembly was utilized to compact approximately 1.5 grams of processed powder into each cylindrical compact with a 0.7 aspect ratio.

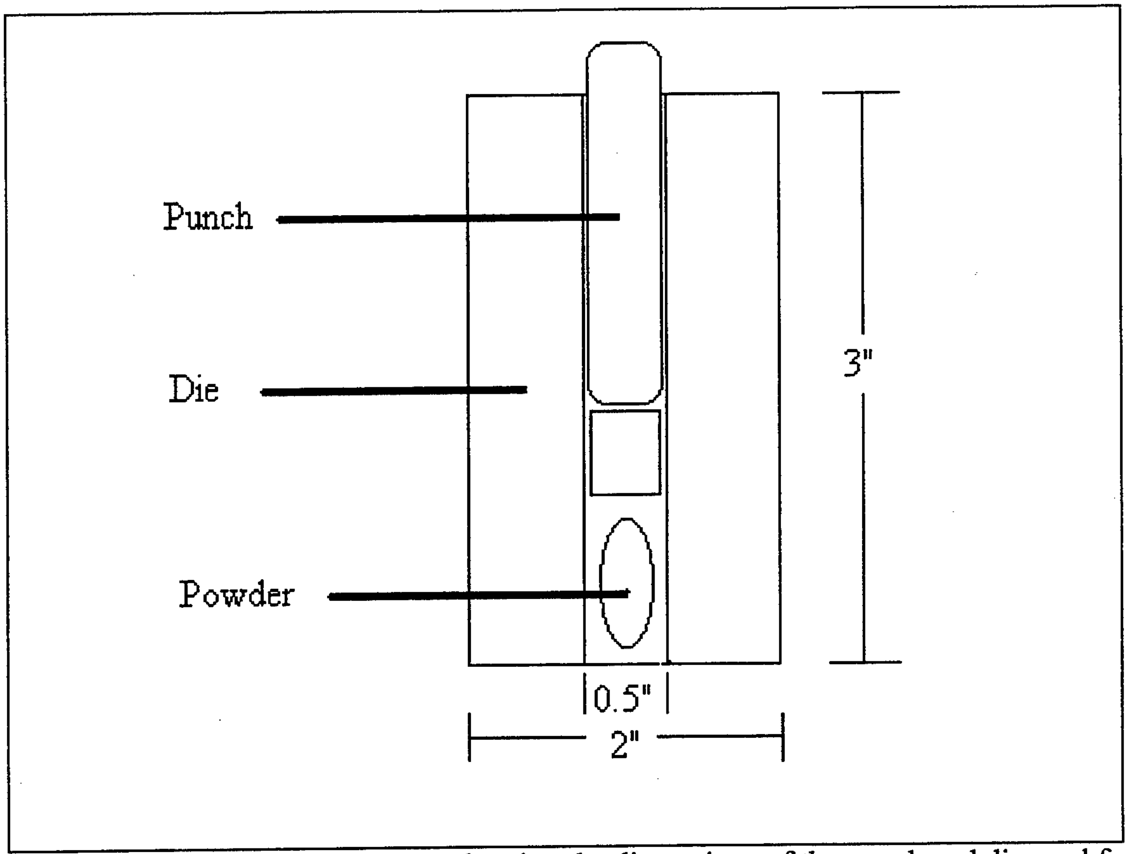

Figure 4.2. A schematic diagram showing the dimensions of the punch and die used for making powder compacts.

The consolidation of the powder compacts was performed by using the punch and die assembly with a SATEC^{TM} model 20UD materials testing system. The SATEC system was programmed to maintain a constant pressure of 80 MPa on the punch for a period of 2.0 hours at ambient temperature. Following compaction, the compacts were removed from the die utilizing a hand press ejection pin.

2. Liquid Phase Sintering

The compacts were sintered at a temperature of 1200°C to provide for a maximum sintered density of the compacts for subsequent testing. The compacts were placed in a tube furnace with atmospheric control, and oxygen (O_2) was passed through the enclosed tube furnace at a low flow rate to carry off any volatiles emanating from the compacts during sintering. The compacts were heated from room temperature to 400°C at 10°C/min and held at 400°C for 30 minutes to allow the additives (PVA, PEG, zinc-stearate) to decompose and/or sublimate. The temperature was subsequently raised to 1200°C at 10°C/min and held at the sintering temperature for a period of 6 hours.

After the 6 hour sintering period, the oven was shut off and the compact allowed to furnace cool to room temperature. Pre- and Post-sintering densities were determined utilizing Archimedes' principle. All measurements were made on a SARTORIUS analog scale, model 2403. The force measurements in air and ethylene glycol were made and calculations discussed previously were conducted to determine compact densities. The density of the ethylene glycol was provided by the manufacturer and verified by measurements of the weight of 10.0 ml of ethylene glycol in a graduated cylinder. To prevent ethylene glycol from penetrating into the interior of the compacts, the compacts were thinly coated with Vaseline Petroleum Jelly [Ref. 11].

3. Deformation of Liquid Phase Sintered Compacts

A schematic diagram of the testing apparatus is shown in Figure 4.3. The connecting bolts and threaded fasteners were made of construction grade steel. The push rods and pressure plates were constructed from Inconel Alloy X-750. Inconel Alloy X-750 is a precipitation hardened alloy of Nickel and Chromium with Titanium and Aluminum additions [Ref. 4]. The furnace was purchased from Watlow Ceramic Fiber Heaters. The heater is a split tube type with an inner diameter of 5.0 inches, an outer diameter of 9.0 inches and is 18.0 inches in length. It is made of an alumina-silica composition and is

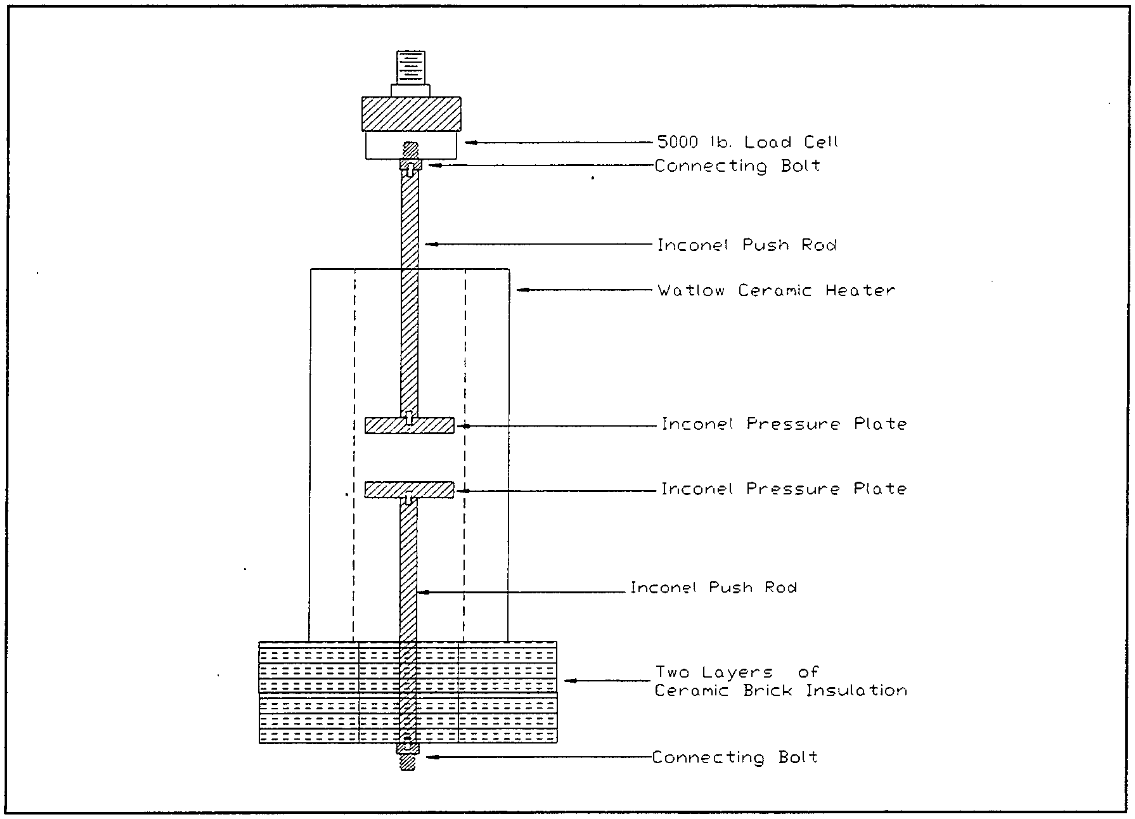
5000 lb. Load Cell
Connecting Bolt
Inconel Push Rod
Watlow Ceramic Heater
Inconel Pressure Plate
Inconel Pressure Plate
Inconel Push Rod
Two Layers of Ceramic Brick Insulation
Connecting Bolt

Figure 4.3. A schematic drawing of the compression assembly (After Ref. 42).

held together by an inorganic binder which allows operation at temperatures up to 1204°C.

The split tube heater was placed on two layers of insulating bricks in order to protect the surface of the testing platform. The top pushrod was fastened to a thermally insulating ceramic that was machined with an outer diameter of 4.5 inches and placed between two steel plates, which was attached to a 5000-pound load cell. The bottom pushrod was attached to the base of the materials testing stand. To provide for lubrication and to reduce surface friction, the surfaces of the Inconel pressure plates were thinly coated with a suspension of MoS_2 and methanol. The plates were allowed to stand at room temperature until the methanol evaporated, leaving a thin layer of MoS_2. Then a suspension of B_2O_3 and cyclohexane was applied on top of the layer of MoS_2. The plates were again allowed to stand at room temperature until the cyclohexane evaporated, leaving a thick layer of B_2O_3 on top of a thin layer of MoS_2. The compacts were targeted and centered on the Inconel pressure plates. A 0.5 inch gap was left between the top of the compact and the top pressure plate to allow for thermal expansion of the system. The heater was then closed and energized.

Two thermocouples were mounted in 1/16" holes on the Inconel pressure plates to monitor the temperature, one on each of the pressure plates. The thermocouples were attached to the heater controller for sensing and feedback. To calibrate the heater controller a bucket of ice water was measured by each thermocouple to ensure proper operation. The system temperature was raised at 3°C/min until a temperature of 900°C was achieved. This temperature was held for 1 hour to achieve steady-state conditions throughout the system. Following equilibration, a compressive load was applied to the compact via the top pressure plate at a nominally constant true strain rate. The load was measured by the 5000-pound load cell. The strain rate was obtained by programming the crosshead velocity as a function of time over 40 discrete time periods. The programmed velocities were determined from the definition of true strain, ε_t:

$$\varepsilon_t = \ln\left(\frac{l_i}{l_o}\right) = \ln\left(\frac{A_o}{A_i}\right) \tag{7}$$

where the height can be related to the cross-sectional area by $A_i l_i = A_o l_o$. Rearranging (7) yields:

$$l_i = l_o e^{\varepsilon_t'} = l_o e^{t\dot{\varepsilon}_t} \quad \textbf{(8)}$$

Taking the derivative as a function of time gives:

$$\dot{\delta} = l_o e^{t\dot{\varepsilon}_t}\dot{\varepsilon}_t \quad \textbf{(9)}$$

where: δ = change in height as a function of time (crosshead veloctiy).
ε_t = change in true strain rate as a function of time.
t = time.
l_o = initial height.

4. X-Ray Diffraction (XRD)

Two compacts were analyzed via XRD. The first compact was sintered at 750°C for 6.0 hours and the second compact was sintered at 1200°C for 6.0 hours. The compacts were ground into fine powder using a mortar and pestle and then mounted on glass slides with amyl-acetate. A goniometer controlled by a DEC VAX workstation was used to examine the samples. The scans were taken from 10° to 100° (2Θ) in increments of 0.05° and time steps of two seconds.

5. Scanning Electron Microscopy (SEM)

The compacts that were prepared for x-ray diffraction were sectioned into two halves using a Buehler series 15 LC diamond wafering blade mounted on an ISOMET^{TM} model 11-1180 low speed saw. The sectioned half of the compact was mounted in a cold-mounted epoxy resin for polishing using a Buehler SAMPL-KIT. The samples were polished using a Buehler model 69-1000 MINIMET polisher/grinder. This polisher was used due to the long polishing times required. The grinding sequence comprised polishing on 320, 400 and 600 grit S_iC paper with Buehler No. 40-8142-128 Polishing Oil for one hour each. Polishing was conducted using 6 μm diamond abrasive on a

TEXMET cloth with Polishing Oil for one hour. Final polishing was conducted using 1 μm diamond abrasive on MICRO-CLOTH with Polishing Oil for one hour. Between each step the sample was placed in a beaker of Polishing Oil in an ultrasonic vibrator to remove any abrasive remaining on the sample surface from the previous step.

When polishing was completed, the Polishing Oil was removed from the samples by rinsing with methanol and the surface dried by heated air at low velocity. The samples were carbon coated by vacuum evaporation and prepared for placement in the scanning electron microscope. The samples were mounted in a Topcon SM-510 Scanning Electron Microscope and studied using both secondary and backscattered electrons.

V. RESULTS AND DISCUSSION

A. POWDER PROCESSING AND SHAPE FORMING

The goal of powder processing is to achieve a particle size distribution that will allow a maximum particle packing that is uniform and free of contaminants, resulting in the highest possible homogeneous density of a green body compact. For the SiO_2-B_2O_3 system, great care was taken in the processing of the powders. Due to the hygroscopic properties of both SiO_2 and B_2O_3, exposure to the atmosphere and any source of water or moisture was minimized prior to the final mixing of the powders [Ref. 43]. To ensure this, the SiO_2 and B_2O_3 powders were each separately ball milled to effect particle size reduction and distribution using cyclohexane and stored in a desicator until mixing. Cyclohexane has no affinity for water and this ensured that there was no agglomeration of the SiO_2 or B_2O_3 particles during the ball-milling process. The final mixture of the powder, with appropriate amounts of SiO_2, B_2O_3, PVA, PEG and zinc stearate was ball-milled and stored in a desicator until compaction. Two powder mixtures were processed using this procedure. The first mixture was composed of SiO_2, 10.0 wt% B_20_3, 3.0 wt% PVA (binder), 3.0 wt% PEG (plasticizer) and 3.0 wt% zinc-stearate (lubricant). The second mixture was composed of SiO_2, 10.0 wt% B_2O_3, 1.0 wt% PVA (binder), 0.5 wt% PEG (plasticizer) and 0.5 wt% zinc-stearate (lubricant).

The object of powder pressing is to form a defect free, homogeneously dense powder compact. The pressing pressure should be high enough to impart sufficient strength for subsequent handling but low enough to avoid excessive wear on the press and tooling [Ref 12]. The prepared powders were formed into cylindrical compacts with an aspect ratio of 0.7 using a punch and die press. The internal walls of the die press were coated with Molybdenum Di-sulfide (MoS_2) to provide lubrication to reduce die-wall friction. The lubricant minimized die-wall friction which aided in the uniform packing of the powder particles throughout the green body powder compact. Variables in the compaction process included the compaction pressure and the time duration that the compaction pressure was applied.

As shown in Table 5.1, a higher relative density was obtained by increasing the compaction pressure. This is in agreement with current research as green density and compact strength increase with increasing pressure [Ref. 12]. By increasing the compaction pressure from 80 to 150 MPa, a relative density increase of 5.1% was observed. However, the change resulted in large internal cracks as shown in Figure 5.1. The large internal cracks originate in the upper corner of the compacts and penetrate inward and downward until they meet, resulting in an elliptic shape as shown in Figure 5.2.

SAMPLE	wt % B_2O_3	$P_{compaction}$ (MPa)	$\rho_{theoretical}$ (g/cm^3)	ρ_{green} (g/cm^3)	$\rho_{relative}$ (g/cm^3)
1	10	80	2.292	1.296	56.6
2	10	120	2.292	1.361	59.4
3	10	150	2.292	1.414	61.7

Table 5.1. Table showing green body densities of compacts as a function of compaction pressure.

Internal cracking has been intensively studied. Critical relationships between die geometry, die-wall friction, and density uniformity of a pressed powder compact are well recognized. However, quantifying these complex relationships and predicting their effects have been difficult [Ref. 12]. Managing friction is critical to successful pressing. Friction between the powder and die wall decreases the pressure available for compaction with increasing distance from the pressing punch. Compact density is directly related to forming pressure. A forming pressure gradient becomes a density gradient in the compact. Density gradients are undesirable because they promote differential densification. Along with density gradients and die-wall friction, the ejection of a compact from the forming die is influenced by elastic springback. Excessive elastic springback can produce catastrophic flaws within the compact. As evidenced in Figure

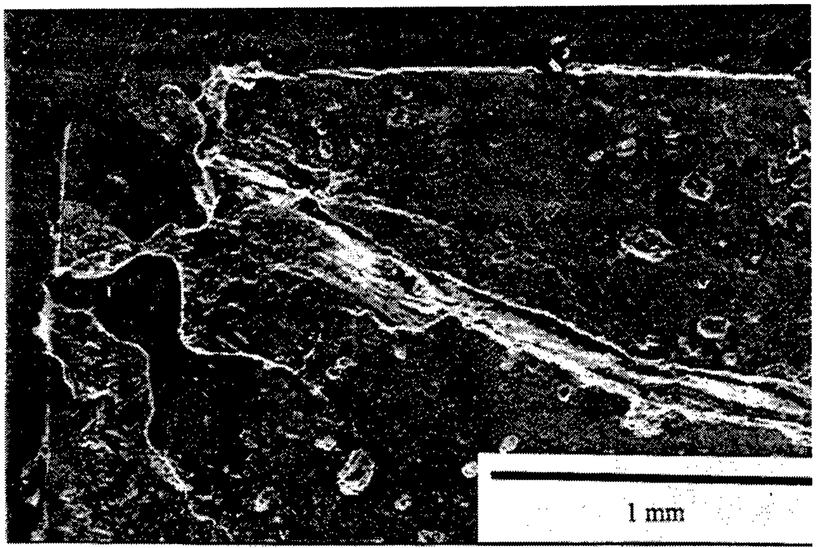

Figure 5.1. SEM micrograph of green body internal cracking (End Capping) in upper left corner of compact.

5.1, End Capping is a central cone-shaped separation that forms at the pressing punch face. It is present throughout the entire compact and has a shape as shown in Figure 5.2.

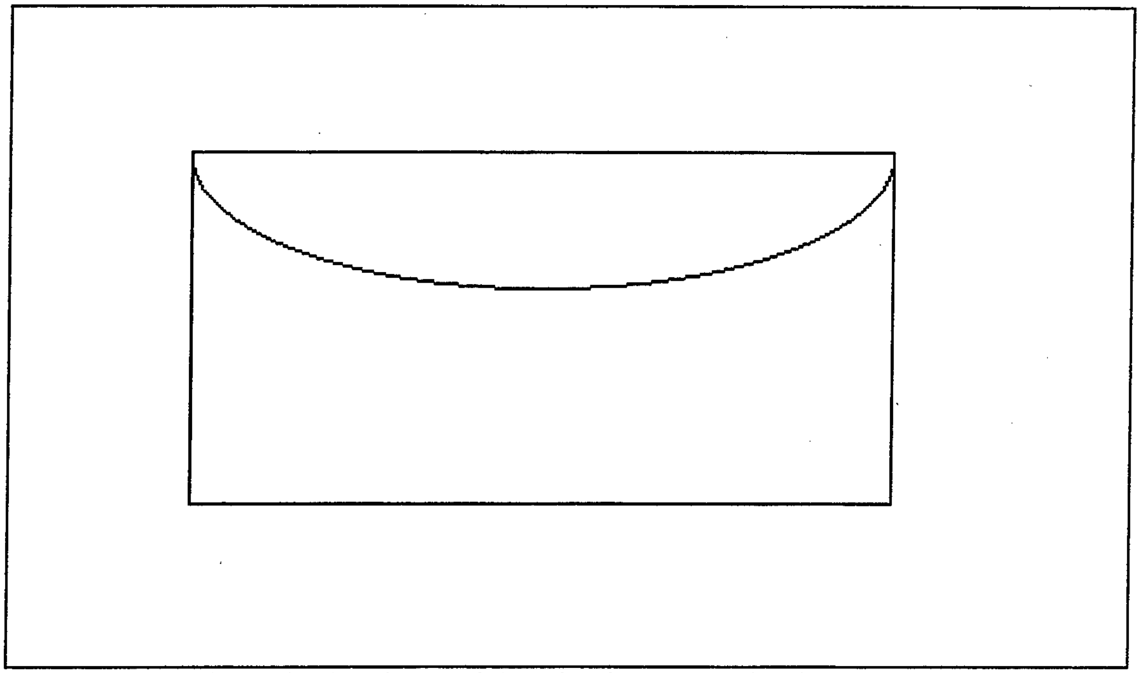

Figure 5.2. Schematic showing End Capping in a green density compact. (After Ref. 4)

It is common in bodies having poor green strength and high springback. High die-wall friction and high pressing pressure contribute to the production of this defect [Ref. 5].

Die-wall friction can be minimized with smooth surface dies, lubricants and low aspect ratio compacts, but it cannot be completely eliminated. Die-wall friction and elastic springback are both reduced by lowering the compaction pressure. Due to the small change in density with increased compaction pressure and the requirement to minimize internal defects, a compaction pressure of 80 MPa was used.

The duration for which the compaction pressure was applied was another variable considered. As shown in Table 5.2, as the time of compaction was increased, the relative density also increased. By increasing the time of compaction from 1 to 16 hours, a 5.2% increase in relative density was observed. This being a relatively small change, a time of two hours was used for the present experiments.

SAMPLE	wt % B_2O_3	Time of Compaction (hr)	$P_{compaction}$ (MPa)	$\rho_{theoretical}$ (g/cm^3)	ρ_{sinter} (g/cm^3)	$\rho_{relative}$ (%)
1	10	1	80	2.630	1.593	60.6
2	10	2	80	2.630	1.618	61.5
3	10	5	80	2.630	1.667	63.4
4	10	16	80	2.630	1.720	65.8

Table 5.2. Table showing densities of sintered compacts as a function of compaction time.

B. SINTERING

1. Density Measurements of Sintered Compacts

With the powder compacts formed, the next step was to sinter the compacts. Variables that were changed were the amount of additives and the temperature at which sintering occurred. As shown in Table 5.3, a higher relative density was obtained with a higher sintering temperature. Also observed was that as the weight percent of additives decreased, the relative density increased.

For densification to occur, it is essential to have (1) an appreciable amount of liquid phase, (2) an appreciable solubility of the solid in the liquid, and (3) wetting of the solid by the liquid [Ref. 39]. Requirements (1) and (2) are met as shown by the 10 wt % B_2O_3 contained in the powder mixture as shown on the phase diagram in Figure 4.1. Requirement (3) is dependent on the nature of the liquid B_2O_3 phase. One of the principal difficulties in the SiO_2-B_2O_3 system is the high viscosity of the liquid phase [Ref 43]. The viscosity of the pure B_2O_3 is shown in Figure 5.3. It is shown in Figure 5.3 that the viscosity of B_2O_3 decreases with increasing temperature. This increases the ability of the solid phase particles to move easily and be packed efficiently via particle rearrangement (the first stage of LPS). The higher temperature also assists by enhancing diffusion and therefore the rate of solution and reprecipitation of the solid phase. Thus, a substantially greater extent of sintering occurs at a higher temperature.

SAMPLE	wt % B_2O_3	ADDITIVES (Mixture)	Tsinter (°C)	$\rho_{theoretical}$ (g/cm^3)	ρ_{sinter} (g/cm^3)	$\rho_{relative}$ (g/cm^3)
1	10	3.0% PVA	750	2.630	1.618	61.5
		3.0% PEG				
2	10	3.0% Zn-Stearate	1200	2.630	1.924	73.2
3	10	1.0% PVA	750	2.630	1.703	64.8
		0.5% PEG				
4	10	0.5% Zn-Stearate	1200	2.630	2.164	82.3

Table 5.3. Table showing densities of sintered compacts as a function of sintering temperature and amount of additives (PVA = polyvinyl alcohol, PEG = polyethylene glycol and Zinc Stearate).

As the amount of additives was decreased, the density increased. This occurred because there were excessive amounts of additives in samples (1) and (2) [Ref. 2].

During the heating cycle, the additives are lost via decomposition and sublimation, leaving voids remaining in the compact. At the burnoff temperature of 400°C, the B_2O_3 has not formed a liquid phase and particle rearrangement does not occur to eliminate the voids. Thus a sufficient amount of additives must be added to provide for lubrication and green body strength, but small enough to prevent excessive voids from remaining due to loss of volatile additives. The highest density achieved was at 1200 °C and was 82.3% of the theoretical density. Compacts sintered at 1200 °C were used in all subsequent experiments.

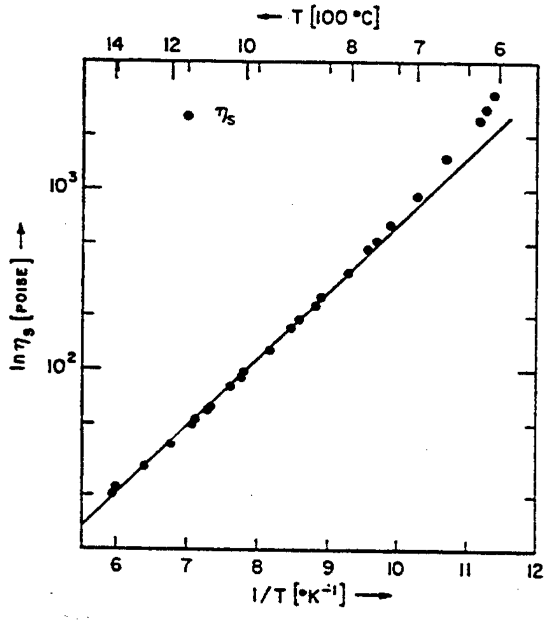

Figure 5.3. Pure B_2O_3 viscosity data as a function of temperature and an Arrhenius fit to the viscosity data. Observe the decrease in viscosity with increasing temperature (After Ref. 44).

It is known that the best sintering techniques cannot overcome problems inherent to the green microstructure such as low green density, agglomeration, and major voids Ref. 9]. The principal difficulties in the SiO_2-B_2O_3 system are the volatization of B_2O_3, the hydration of SiO_2-B_2O_3 mixtures, and the high viscosity of SiO_2-B_2O_3 melts [Ref. 43]. The volatization of pure B_2O_3 is shown in Figure 5.4. It is clearly seen that the wt% of B_2O_3 decreases with time while at high temperatures. As B_2O_3 volatizes in the compact, it can form pores (voids) and result in an ever-decreasing amount of B_2O_3 which is needed to support liquid phase sintering. Thus, volatization of B_2O_3 effects a reduction in the final sintered density.

The hydration of the SiO_2-B_2O_3 mixture causes agglomeration of the powder during the powder mixing process. This prevents the B_2O_3 from achieving a uniform distribution throughout the powder mixture, which results in an uneven distribution of B_2O_3 in the compact. During sintering, in regions without B_2O_3 at the grain boundaries, solid state sintering will occur, forming a rigid solid skeleton which will inhibits further densification.

As shown in Figure 5.3, the viscosity of B_2O_3 is very high for most of the temperature range [Ref. 45]. With higher temperatures, the viscosity decreases, aiding densification. However, at higher temperatures the volatization of B_2O_3 is increased and as mentioned previously, this causes a reduction in the final sintered density. Thus, in the SiO_2-B_2O_3 system, achieving a high final sintered density can be difficult due to the properties of the system.

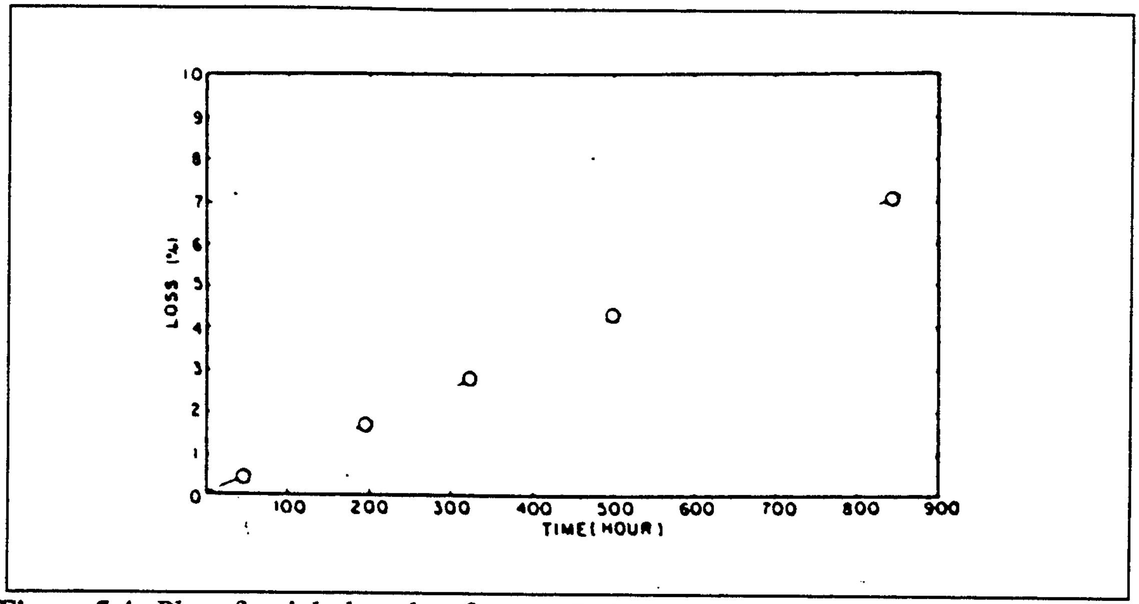

Figure 5.4. Plot of weight loss data for pure B_2O_3 at 730°C (From Ref. 43).

2. X-Ray Diffraction of Sintered Compacts

Analysis of the sintered compacts was performed using x-ray diffraction (XRD). As shown in Figure 5.5, the diffraction patterns produced by a sintered compact at 750 °C are the same as the Joint Committee on Powder Diffraction Standards (JCPDS) for a combination of SiO_2 quartz and B_2O_3. The diffraction pattern for SiO_2 quartz is the same as listed on JCPDS card number 33-1161. The diffraction pattern for B_2O_3 is for B_2O_3 80C, a cubic polytype of boron oxide, and is listed on JCPDS card number 6-0297. From the phase diagram of the SiO_2-B_2O_3 system (Figure 4.1), this is what was expected.

The diffraction pattern produced by a sintered compact at 1200 °C is shown in Figure 5.6. This diffraction pattern reveals a combination of SiO_2 quartz, SiO_2 tridymite and B_2O_3. The JCPDS card numbers are the same for SiO_2 quartz and B_2O_3, and for SiO_2 tridymite is 18-1170. Again, from the phase diagram (Figure 4.1), this is what was expected. The relative amounts of quartz and tridymite are unknown as tridymite is a metastable form of quartz at room temperature, with the re-transformation into quartz occurring slowly.

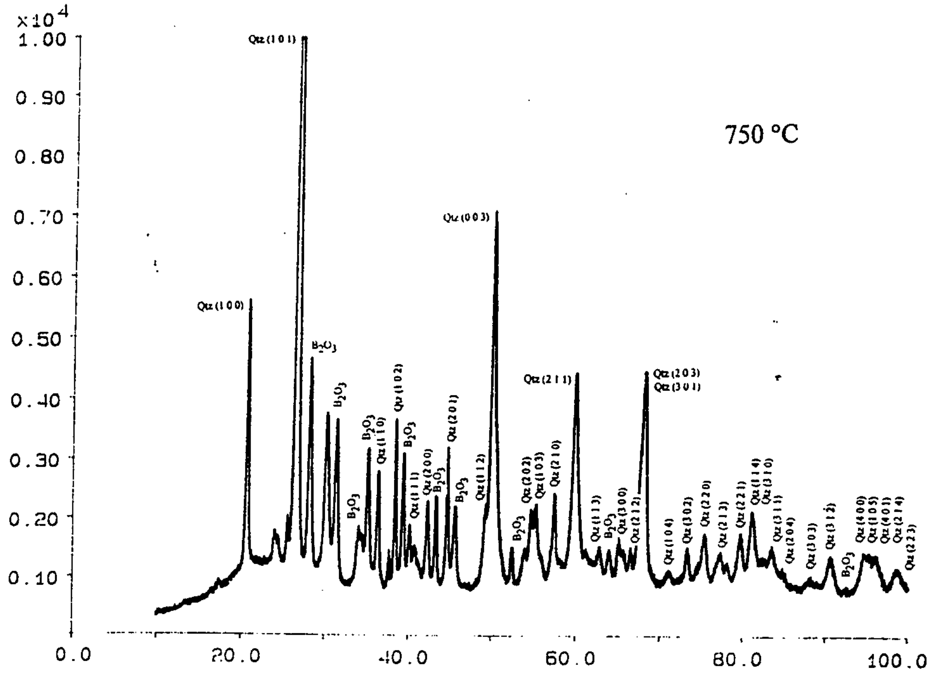

Figure 5.5. X-Ray diffraction pattern of SiO_2-B_2O_3 at 750°C for six hours.

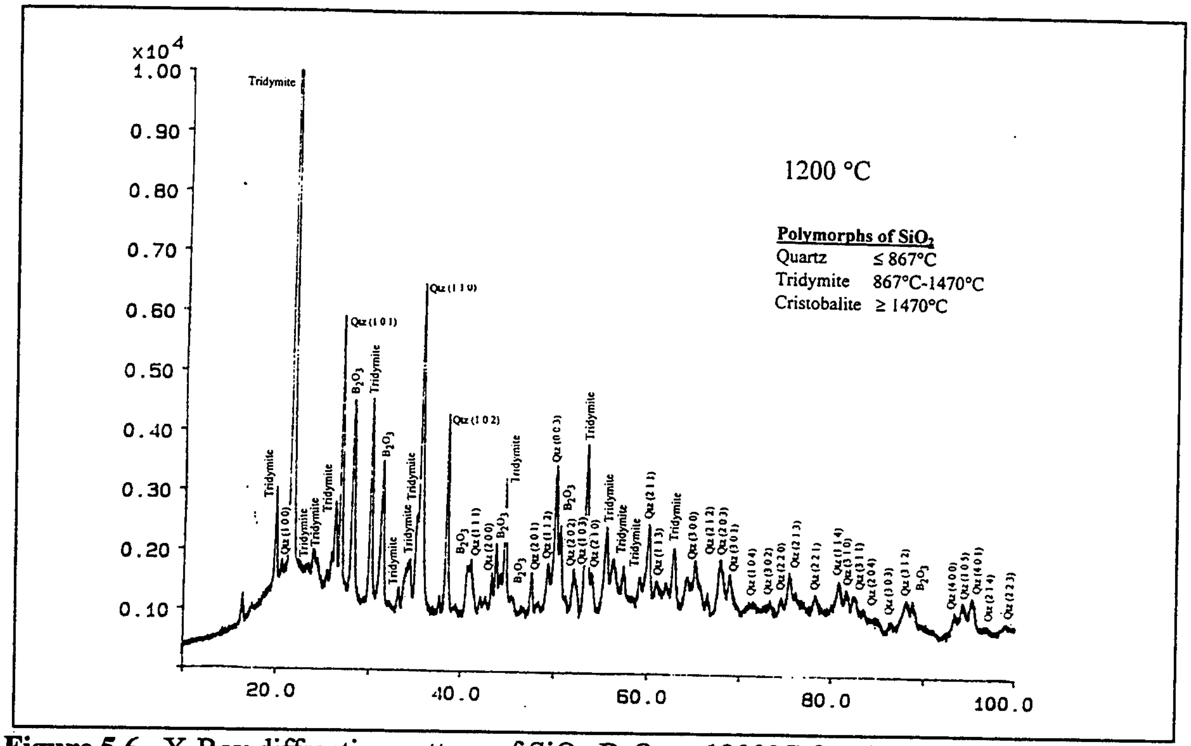

Figure 5.6. X-Ray diffraction pattern of SiO_2-B_2O_3 at 1200°C for six hours.

3. Scanning Electron Microscopy of Sintered Compacts

Scanning electron microscopy was performed on a compact sintered at 1200 °C. As seen in Figures 5.7 and 5.8, there are large and small voids with small internal cracks throughout the sample. The remaining areas of the sample are regions that are partially and fully sintered.

The voids are attributed to the trapping of the gaseous B_2O_3 after evaporation [Ref. 1]. The volatization rate of B_2O_3 is shown in Figure 5.4 and is verified by the X-ray diffraction data shown in Figures 5.5 and 5.6. The B_2O_3 peaks are weaker at 1200°C than at 750°C, thus accounting for a loss of B_2O_3 due to volatization at the higher temperature. Inside the compact, the gaseous products can become trapped if the equilibrium pressure of the pore/void is exceeded due to the small size of the pore/void. In regions where there is not a sufficient amount of liquid phase to enhance diffusion, the gaseous products become trapped by the solid skeleton. As the B_2O_3 evaporates, regions of the compact will have deficient amounts of B_2O_3 and will not be able to support liquid phase sintering and the accompanying diffusion mechanisms. This defect is common where high heating rates are used and where there is a temperature gradient between the surface and the interior [Ref. 1]. Thus, the pore becomes sealed, trapping the gaseous products inside the compact to form a void.

An additional cause of voids can be attributed to nonuniform mixing of the initial powder prior to compaction. This is one of the most important reasons why densification shrinkage stops short of complete elimination of the pores. Nonuniform mixing induces local variations in density during forming, causing voids to form. This is the initial porosity that is present following compaction. These voids tend to become trapped in the compact during sintering [Ref. 1].

Small cracks are also evident in Figures 5.7 and 5.8. These cracks are due to residual stresses from compaction and induced stresses due to phase transformations. During the compaction process, density gradients are produced throughout the compact. High-density areas densify faster than low-density areas, which produce stresses due to the warpage and volume changes [Ref. 12]. These stresses produce cracking. Another cause of cracking is due to the two phase transformations that occur during the heating and cooling cycles [Ref 1]. As previously discussed, there is a displacive transformation from low quartz to high quartz at 573°C and this occurs with a volume change of 1.6%

[Refs. 1 and 2]. At 867°C, quartz transforms into tridymite. The induced stresses due to the volume changes also cause cracking.

Analysis of Figures 5.9 and 5.10 show the particle size and the particle size distribution of the mixed powder prior to compaction. Some of the particles have agglomerated and it is difficult to distinguish individual particles in some areas. As can be seen the particle size is in the range of approximately 0.1-0.5 μm with a distribution of particle sizes. It is known that the ideal starting material to fabricate a fine-grained ceramic is a small-sized (0.1 to 1.0 μm), equiaxed powder with a narrow size distribution [Ref. 10].

Figures 5.11 through 5.14 are pictures of regions for comparison between scanning electron and backscatter images. It can be seen that the grain size is approximately 1.0 μm. In Figures 5.12 and 5.14, small amounts of B_2O_3 are present as small white circles at the grain junctions. It is also seen that in the backscatter mode that there is sufficient B_2O_3 throughout the compact to provide for liquid phase sintering. B_2O_3 (atomic number Z=34) is shown as the "white" regions and SiO_2 (Z=30) is shown as the "black" regions in the backscatter images. These figures indicate that there is significantly more B_2O_3 in the compact than that needed to produce liquid phase sintering, resulting in the large accumulation of B2O3 in the intergranular regions. Some excess B_2O_3 will be required because B_2O_3 volatizes at elevated temperatures [Ref. 31]. Excess B_2O_3 will volatize and form voids when trapped in the interior of the compact as discussed previously. However, it should be possible to optimize the amount of B_2O_3 to provide for Liquid Phase Sintering and to minimize the production of voids.

From the SEM images, all of the reasons for having only an 82.3% theoretically dense sample were clearly seen. The internal cracks, voids and regions of incomplete sintering prevented the formation of a sintered product with near-theoretical density. The samples with the highest densities produced following sintering at 1200°C were then subjected to mechanical testing.

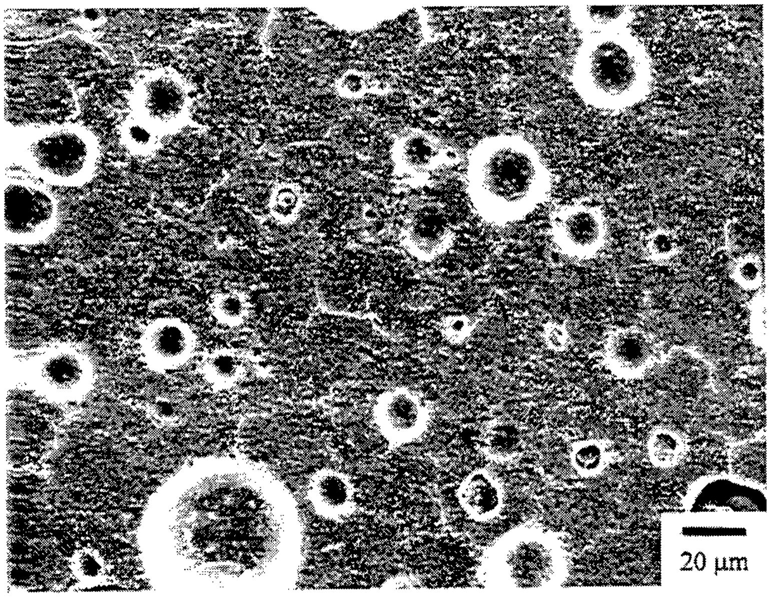

Figure 5.7. SEM micrograph of a sectioned compact sintered at 1200°C for six hours. Note the large numbers of voids and small internal cracks.

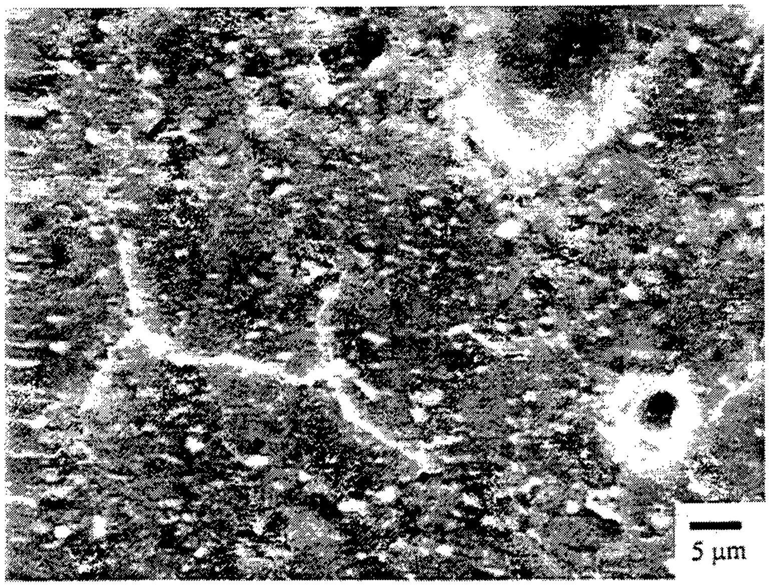

Figure 5.8. SEM micrograph of a sectioned compact sintered at 1200°C for six hours. Note the internal crack and large and small voids.

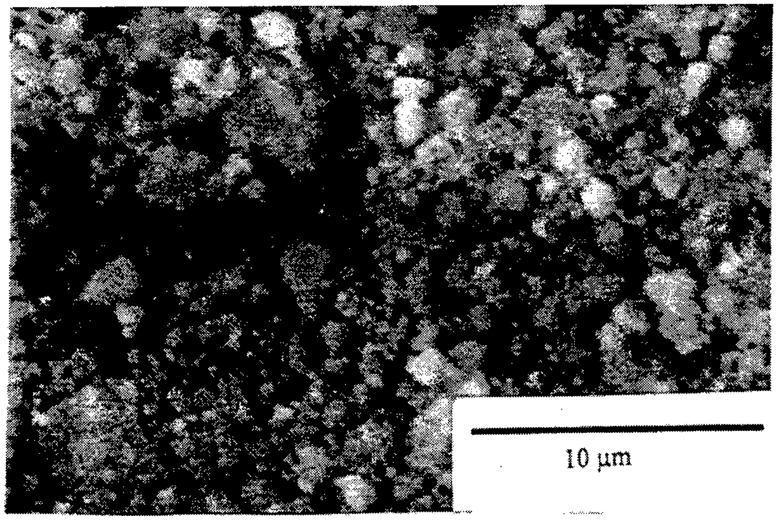

Figure 5.9. SEM micrograph of powder mixture prior to compaction. Powder mixture is SiO_2, 10 wt% B_2O_3, 1.0 wt% PVA, 0.5 wt% PEG and 0.5 wt% Zn-stearate. Note the average particle size and particle size distribution.

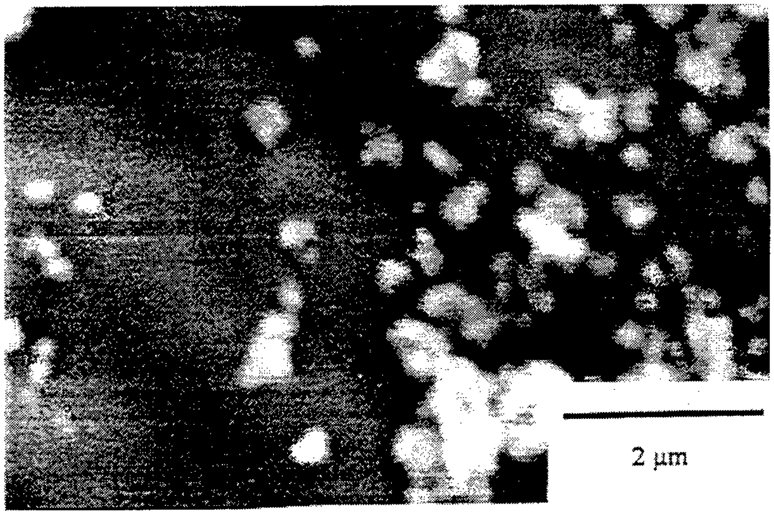

Figure 5.10. SEM micrograph of powder mixture prior to compaction. Powder mixture is SiO_2, 10 wt% B_2O_3, 1.0n wt% PVA, 0.5 wt% PEG and 0.5 wt% Zn-stearate. Note the size of the individual particles.

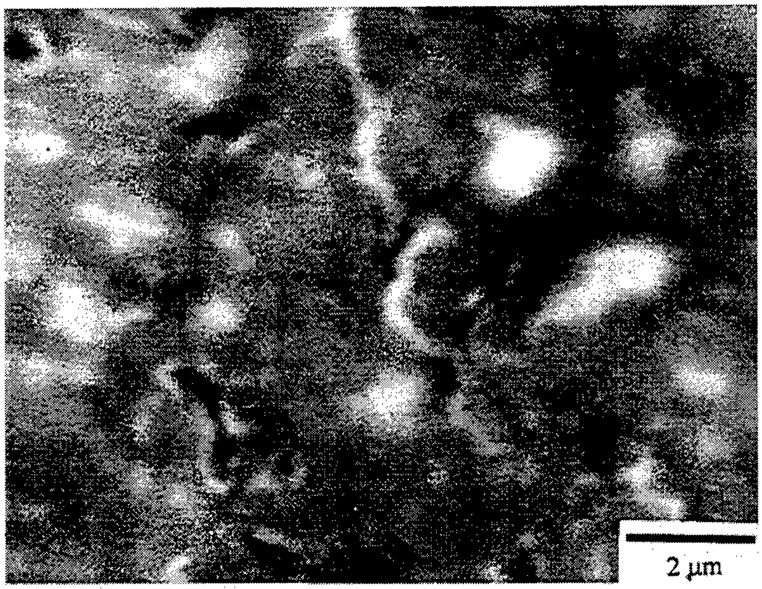

Figure 5.11. SEM micrograph of a sectioned compact sintered at 1200°C for six hours. Note the small inter-particle voids and grain size.

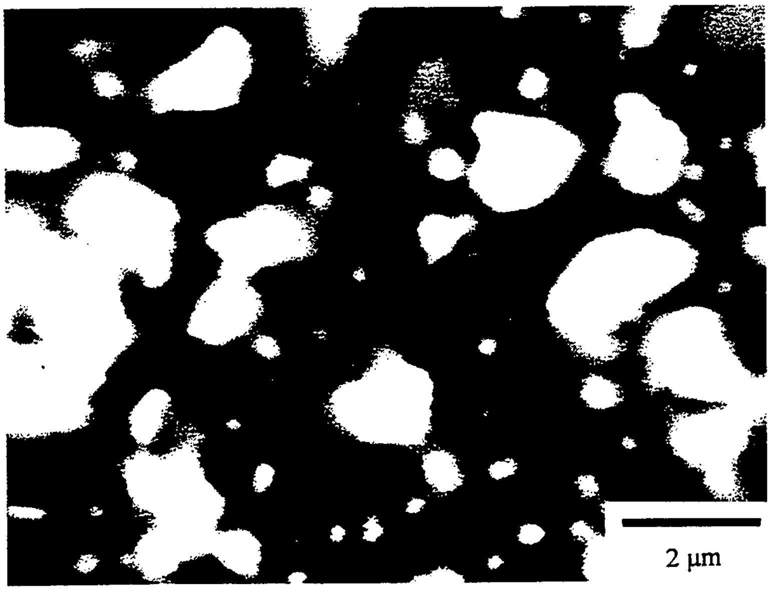

Figure 5.12. SEM back-scatter micrograph of a sectioned compact sintered at 1200°C for six hours. Note the accumulations of B_2O_3 (white, Z=34) between the SiO_2 particles (black, Z=30). Compare to scanning electron (SE) mode in Figure 5.8.

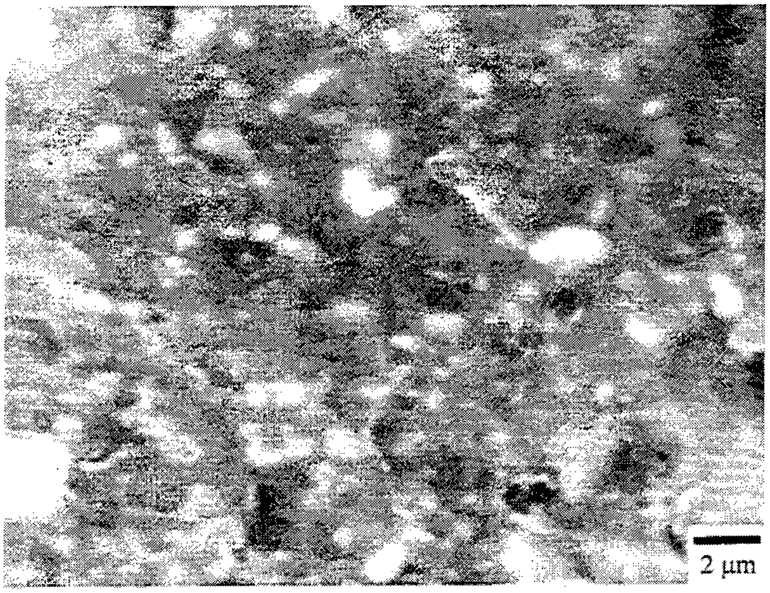

Figure 5.13. SEM micrograph of a sectioned compact sintered at 1200°C for six hours. Note the sintered regions with very little porosity.

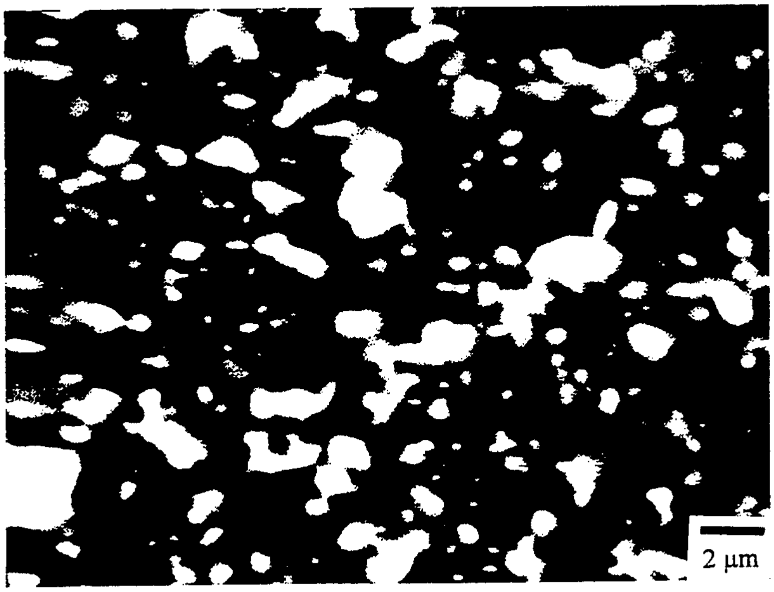

Figure 5.14. SEM back-scatter micrograph of a sectioned compact sintered at 1200°C for six hours. note the accumulations of B2O3 (white, Z=34) between the SiO2 particles (black, Z=30). Compare to Scanning electron (SE) mode in Figure 5.10.

C. DEFORMATION OF THE SINTERED COMPACT

Deformation of some compacts was performed using the compression apparatus described in Figure 4.3. The crosshead velocity was programmed as a function of strain so that a nominally constant true strain rate could be maintained for the duration of the test. Compression tests were conducted up to total pre-set strains of either 25% or 35% because of limitations in the design of the test apparatus. All test were conducted at 900°C at a strain rate of $5x10^{-4}$ s^{-1}. This is shown in Figure 5.15, which plots the nominal true stress vs. the nominal true compressive strain. Following the initial elastic deformation, the curves are observed to decrease in slope rapidly. Although the curves do not flatten out to a near-zero slope, as would be expected in true superplasticity, it is to be realized that the tests were not continued to large strains because of apparatus limitations. The maximum permanent deformation induced in the samples (as measured following extrication of the sample from the fixtures after deformation) was around 20%. No damage was observed in the samples at this point.. Figures 5.16 and 5.17 show a typical compact prior to, and following deformation. It is possible that if the tests were to be continued beyond the present 35%, the stress-strain curve would flatten out, and exhibit a more superplastic-like behavior.

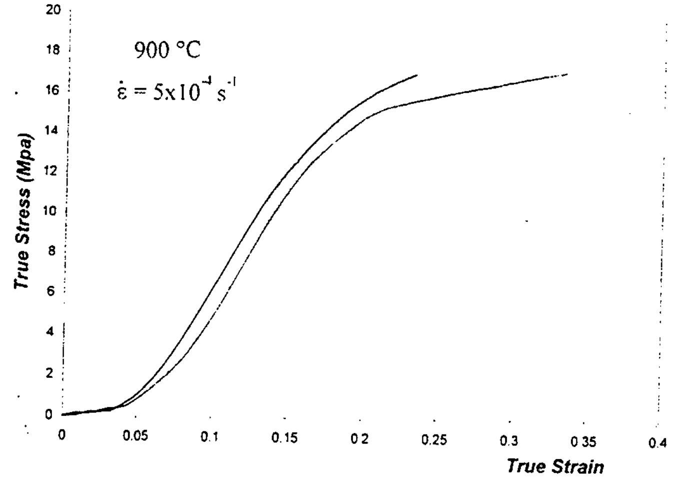

Figure 5.15. Plot of nominal true stress vs. true strain for the SiO_2-B_2O_3 compacts. Both tests were performed at a temperature of 900°C and a nominally constant true strain rate of $5\times10^{-4}\ s^{-1}$.

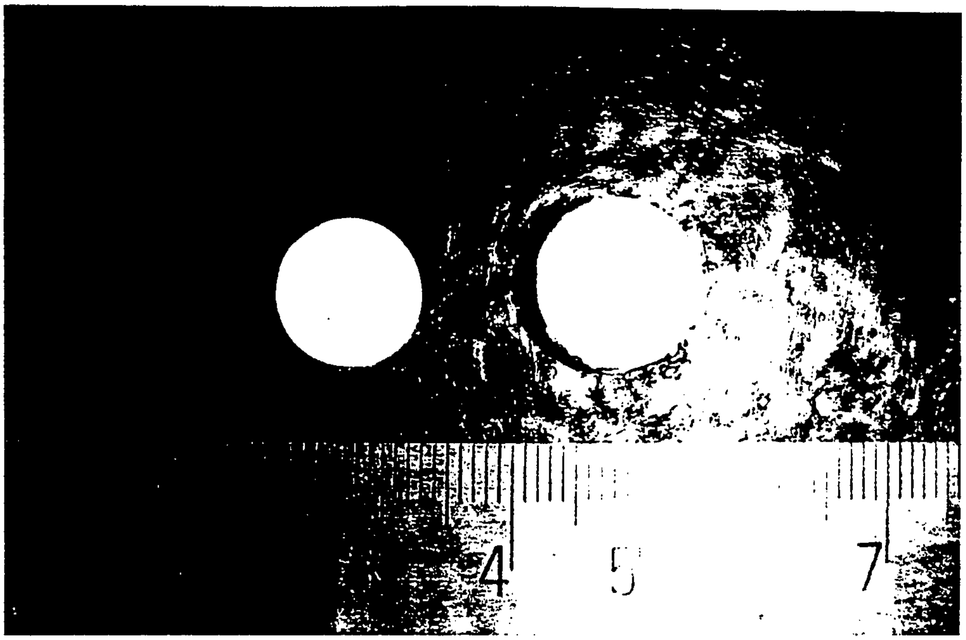

Figure 5.16. Picture of a sintered compact next to a compact that underwent ~20% deformation (top view).

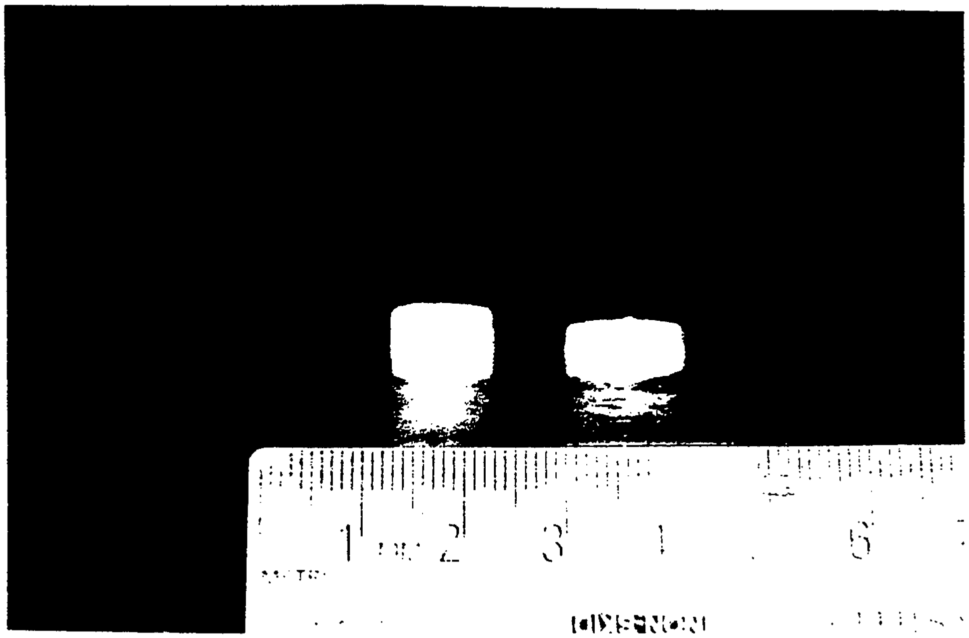

Figure 5.17. Picture of a sintered compact next to a compact that underwent ~20% deformation (side view).

Due to the evidence that the solution-reprecipitation mechanism was active during Grain Shape Accommodation in sintering, it is suggested that the same mechanism was active during deformation as Grain Boundary Sliding. Post-deformation density of deformed compacts revealed around 80% of the theoretical density. Thus, it is clear that there was no significant densification during the compression test. Therefore, the observed plastic strain is due to actual deformation of the compact, and not due to additional compaction and sintering under the high-temperature upsetting conditions prevalent during the tests. The slightly decreased density is probably attributable to the increase in the properties of tridymite relative to quartz due to polymorphic tranformations during the test (tridymite has a lower density, $\rho_{tridymite}$=2.26 g/cm^3 than quartz, ρ_{qtz}=2.64 g/cm^3). Therefore, the deformation is suggested to be mostly due to Grain Boundary Sliding (GBS).

VI. CONCLUSIONS AND RECOMMENDATIONS

The goals of this study were to evaluate the SiO_2-B_2O_3 model system for suitability for Liquid Phase Sintering and to perform a preliminary investigation of the deformation behavior of the system above its melting point. Scanning Electron Microscopy (SEM) and X-Ray Diffraction Analysis (XRD) were used to analyze the sintered compacts. Deformation of a compact at elevated temperature demonstrated ~20% deformation in the presence of a liquid phase.

Significant progress was achieved in the ability to form a dense compact. However, higher densities are required in order to take advantage of deformations concurrent with liquid phase sintering, especially under tensile conditions, where internal voids can lead to strain localization and premature failure. SEM analysis showed voids and some microcracks in various locations within the compacts. The cracks, which were very small, were attributed to internal stresses caused by phase transformations. The voids are probably attributable to an excess of B_2O_3 and its evaporation at the sintering temperature of 1200°C. It is recommended that a further refinement of the powder processing method be undertaken to include a better mixture of polyvinyl alcohol, polyethylene glycol and zinc stearate to produce less volatiles when heated and a reduction in the amount of B_2O_3 to that amount which is just sufficient to support Liquid Phase Sintering. With a more thoroughly mixed powder, a lower sintering temperature may be achieved with a reduction of the internal defects.

The ability to significantly deform the compact was demonstrated. A minimum of ~20% permanent strain was obtained. Further deformation is possible but was precluded by limitations in the testing apparatus design. There was significant friction between the compact and the compression surfaces that hindered the ability of the compact to freely deform and the testing apparatus was limited to a moderately high temperature. It is therefore recommended that for future tests, a fine layer of borosilicate glass fiber be used to lubricate the compression surfaces to minimize friction between the compression plates and the compact and the testing apparatus be modified to allow testing at higher temperatures.

It is difficult to achieve high sintered densities in the SiO_2-B_2O_3 system, as evidenced by the extensive literature devoted to research on this system. However, if the inherent problems encountered with this system can be overcome, this would be an excellent model system. In the event these limitations cannot be overcome, alternative Liquid Phase Sinter Forming model systems could be explored. Systems with Al_2O_3 and Bi_2O_3 show promise with a low melting temperature phase. Therefore, it is recommended that if the problems with the SiO_2-B_2O_3 system cannot be corrected, an alternative model system be chosen.

LIST OF REFERENCES

1. Kingery, W. D., H.K. Bowen and D. R. Uhlmann., *Introduction to Ceramics. 2nd ed.*, John Wiley and Sons, Inc., 1976.

2. Richerson, David W., *Modern Ceramic Engineering, Properties, Processing and Use in Design.* 2nd ed., Marcel Dekker Inc., 1992.

3. Lenel, F. V. *Powder Metallurgy, Principles and Applications*. Metal Powder Industries Federation, 1980.

4. Klar, Erhard, ed., *Metals Handbook.* American Society for Metals, 1984.

5. Glass, S. J. and K. G. Ewsuk, "Ceramic Powder Compaction," *MRS Bulletin*, December 1997.

6. Neih, T. G., J. Wadsworth and F. Wakai., "Recent Advances in Superplastic Ceramics and Ceramic Composites." *International Materials Review*, **36**: pp. 146-161, 1991.

7. Samuneva, B., P. Vinarov and M. Dimitrova., "Processes for Silica Glass Powder Sintering." *Journal of Non-Crystalline Solids*, **112**: pp. 198-203, 1989.

8. German, Randall M. *Sintering Theory and Practice*. John Wiley and Sons, Inc., 1996.

9. Pharr, G. M. and M. F. Ashby, "On Creep enhanced by a Liquid Phase," *Acta. Metall.*, **31**: p.129, 1983.

10. Jubb, N. J. and H. K. Bowen, "The Processing of Monodisperse Boron-doped SiO_2 Particles," *Journal of Materials Science*, **22**: p. 1987.

11. Blumenthal, W. R., H. Sheinberg and S. A. Bingert., "Compaction Issues in Powder Metallurgy," *MRS Bulletin*, December 1997.

12. Ewsuk, K. G., "Compaction Science and Technology," *MRS Bulletin*, December 1997.

13. Huang, Ching-Yao and G. S. Daehn, "Densification of Composite Powder Compacts in Pressure Cycling," *Acta Mater.*, **44**: pp. 1035-1045, 1996.

14. Kim, Kitae T. and G. Son, "Cyclic Compaction of Ceramic Powders," *J. Am. Ceram. Soc.*, **75**: pp. 3157-3159, 1992.

15. Streeter, V. L. and E. B. Wylie, *Fluid Mechanics*, McGraw-Hill Publishing, Inc., 1985.

16. Clasen, R., "Preparation and Sintering of High-Density Green Bodies to high-Purity Silica Glasses," *Journal of Non-Crystalline Solids*, **89**: pp. 335-344, 1987.

17. Chokshi, A. H., A. K. Mukherjee and T. G. Langdon., "Superplasticity in Advanced Materials," *Materials Science and Engineering*, **R10**: pp. 237-274, 1993.

18. Maehara, Y. and T. G. Langdon, "Review Superplacticity in Ceramics," *Journal of Materials Science*, **25**: pp. 2275-2286, 1990.

19. Nieh, T. G. and J. Wadsworth. "The Role of Liquid Phase on Superplasticity in Metals and Ceramics," *Materials Science Forum*, **233-234**: pp. 383-398, 1997.

20. Nieh, T. G., J. Wadsworth and F. Waikai., "Recent Advances in Superplastic Ceramics and Ceramic Composities," *International Materials Review*, **36**: pp. 146-161, 1991.

21. Wakai, F., N. Kondo, H. Ogawa, T. Nagano and S. Tsurekawa., "Ceramics Superplasticity: Deformation Mechanisms and Microstructures," *Materials Characterization*, **37**: pp. 331-334, 1996.

22. Nieh, T. G. and J. Wadsworth, "Effect of Grain size on Superplastic Behavior of Al_2O_3/YTZ," *Journal of Materials Research*, **5**: p. 2510, 1990.

23. White, Frank, *Fluid Mechanics*, McGraw-Hill Inc., 1994.

24. Courtney, Thomas H., *Mechanical Behavior of Materials*, McGraw-Hill Publishing, New York, 1990.

25. Valeiv, R. Z. and O. A. Kaibyshev, "On the Quantitative Evaluation of Superplastic Flow Mechanisms," *Acta Metall.*, 31: pp. 2121-2128, 1983.

26. Langdon, T. G., "An Evaluation of the Strain Contributed by Grain Boundary Sliding in Superplasticity," Departments of Materials Science and Mechanical Engineering, University of Southern California, 1993.

27. Arzt, E., M. F. Ashby and R. A. Verral, "Interface-Reaction-Controlled Diffusional Creep," *Acta Metall.*, **31**: pp. 1977-1989, 1983.

28. Ashby, M. F. and R. A. Verral, "Diffusion-Accomodated Flow and Superplasticity," *Acta. Metall.*, **21**: pp. 149-163, 1973.

29. Chaudhury, P. K, and F. A. Mohamed, *Acta. Metall.*, **36**: 1099, 1988.

30. Valiev, R. Z, and T. G. Langdon, *Acta Metall.*, **41**: 949, 1993.

31. Cannon, W. R. and T. G. Langdon, *J. Mater. Sci.*, **23**: 1, 1988.

32. Raj, R., R. L. Tsai, J. G. Wang and C. K. Chyune, "Deformation of Ceramic Materials II," p353, 1984.

33. Nieh, T. G. and J. Wadsworth, "Superplasticity and Superplastic Forming of Ceramics," *Materials Science Forum*, Vols. 170-172, pp. 259-268, 1994.

34. Raj, R. and C. K. Chyung, "Solution-Precipitation Creep in Glass Ceramics," *Acta Metall.*, **23**: pp. 159-166, 1986.

35. Clarke, D. R., "On the Equilibrium Thickness of Intergranular Glass Phases in Ceramic Materials," *J. Am. Ceram. Soc.*, **70**: pp. 15-22, 1987.

36. Schissler, D. J., A. H. Chokshi, T. G. Nieh and J. Wadsworth, "Microstructural Aspects of Superplastic Tensile Deformation and Cavitation Failure in a Fine-Grained Yttria Stabilized Tetragonal Zirconia," *Acta Metall. Mater.*, 39: pp. 3227-3236, 1991.

37. Rockett, T. J. and W. R. Foster, *J. Am. Ceram Soc.*, **48**: p.78, 1965.

38. Calister, William, *Materials Science and Engineering. 2nd ed.*, John Wiley and Sons, Inc., 1991.

39. *Metals Handbook*, Ninth Edition, Vol. 2 Properties and Selection: Nonferrous Alloys and Pure Metals, American Society for Metals, Metals Park, Ohio, 1979.

40. *Metals Handbook*, Ninth Edition, Vol. 4 Heat Treating, American Society for Metals, Metals Park, Ohio, 1981.

41. *Metals Handbook*, Tenth Edition, Vol. 1 Properties and Selection: Irons, Steels, and High-Performance Alloys, Materials Park, Ohio, 1990.

42. Lloyd, M. L., *A Feasibility Study of Liquid Phase Sinter Forming of a Model Ceramic System*, Master's Thesis, Naval Postgraduate School, Monterey, California, September 1998.

43. Rockett, T. J. and W. R. Foster, "Phase Relations in the System Boron Oxide-Silica," *J. Am. Ceram Soc.*, **48**: p.75, 1965.

44. Macedo, P.B. and A. Napolitano, "Inadequacies of Viscosity theories for B_2O_3," *Journal of Chemical Physics*, **49**: pp. 1887-1895, 1968.

45. Charles, R. J. and F. E. Wagstaff, "Metastable Immiscibility in the B_2O_3-SiO_2 System," *J. Am. Ceram Soc.*, **51**: pp. 16-20, 1967.

INITIAL DISTRIBUTION LIST

1. Defense Technical Information Center
   8725 John J. Kingman Rd., STE 0944
   Ft. Belvoir, VA 22060-6218 2

2. Dudley Knox Library
   Naval Postgraduate School
   411 Dyer Rd.
   Monterey, CA 93943-5101 2

3. Professor I. Dutta, Code ME/Du
   Department of Mechanical Engineering
   Naval Postgraduate School
   Monterey, CA 93943 2

4. Professor A. Gopinath, Code ME/Gk
   Department of Mechanical Engineering
   Naval Postgraduate School
   Monterey, CA 93943 2

5. LT Roland C. Roeder
   3201 Rods Drive
   Sandusky, OH 44870 2